Weierstraß-Institut
für Angewandte Analysis und Stochastik

Leibniz-Institut im Forschungsverbund Berlin e. V.

Preprint ISSN 2198-5855

Axisymmetric mass conservative coupling of fluid flow and solute transport

Jürgen Fuhrmann, Christian Merdon, Daniel Runge

submitted: March 3, 2026

Weierstrass Institute
Anton-Wilhelm-Amo-Str. 39
10117 Berlin
Germany
E-Mail: juergen.fuhrmann@wias-berlin.de
christian.merdon@wias-berlin.de
daniel.runge@wias-berlin.de

No. 3264
Berlin 2026

2020 *Mathematics Subject Classification.* 76D07, 65N30, 65N08, 35B45.

2010 *Physics and Astronomy Classification Scheme.* 47.10.ad, 47.11.Df.

Key words and phrases. Transport equation, Stokes equation, cylindrical coordinates, a priori error estimates, maximum principle, mass conservation.

The authors gratefully acknowledge the funding by the German Science Foundation (DFG) within the project “ME 4819/2-1”.

Edited by
Weierstraß-Institut für Angewandte Analysis und Stochastik (WIAS)
Leibniz-Institut im Forschungsverbund Berlin e. V.
Anton-Wilhelm-Amo-Straße 39
10117 Berlin
Germany

Fax: +49 30 20372-303
E-Mail: preprint@wias-berlin.de
World Wide Web: http://www.wias-berlin.de/

Axisymmetric mass conservative coupling of fluid flow and solute transport

Jürgen Fuhrmann, Christian Merdon, Daniel Runge

ABSTRACT. This paper is concerned with the physically consistent simulation of fluid flow and transport in complex geometries axisymmetric geometries. In this situation, cylindrical coordinates allow a dimension reduction of the three-dimensional problem to a two-dimensional one. In the three-dimensional setting, a mass conservative discretization can be achieved, e.g. by coupling divergence-free finite element methods for the flow with a conservative finite volume discretization for the transport. A replication of this approach in the reduced two-dimensional formulation with cylindrical coordinates is not straight-forward. Therefore, modifications are suggested that ensure the desired qualitative properties and allow *a priori* error estimates in suitable weighted Sobolev norms. Several numerical experiments study convergence rates and confirm the theoretical results.

1. INTRODUCTION

This contribution studies the coupling of the velocity field $\widehat{\boldsymbol{u}}$ from the incompressible Stokes equations

$$-\nu\Delta_x\widehat{\boldsymbol{u}} + \nabla_x\widehat{p} = \widehat{\boldsymbol{f}} \tag{1.1}$$

$$\operatorname{div}_x\widehat{\boldsymbol{u}} = 0 \tag{1.2}$$

with the diffusive-convective transport of some species c according to

$$\operatorname{div}_x(\widehat{\boldsymbol{j}}) = \widehat{s} \quad \text{where} \quad \widehat{\boldsymbol{j}} := -D\nabla_x\widehat{c} + \widehat{\boldsymbol{u}}\,\widehat{c} \tag{1.3}$$

under assumptions of axisymmetry and suitable boundary conditions. In particular, we assume that the domain $\widehat{\Omega}$ is obtained by a full revolution around the z-axis of some two-dimensional domain Ω and that the data is such that the problem can be reformulated in cylindrical coordinates (r, z) on Ω with a stripped-off angular dimension. Then, one effectively seeks some two-dimensional velocity field $\boldsymbol{u} = (u_r, u_z)$, and a scalar-valued pressure field p such that

$$-\nu\left(\Delta_{\text{cyl}}u_r - \frac{u_r}{r^2}\right) + \frac{\partial p}{\partial r} = f_r \qquad \text{where } \Delta_{\text{cyl}} := \frac{\partial^2}{\partial r^2} + \frac{1}{r}\frac{\partial}{\partial r} + \frac{\partial^2}{\partial z^2} \tag{1.4}$$

$$-\nu\Delta_{\text{cyl}}u_z + \frac{\partial p}{\partial z} = f_z \tag{1.5}$$

$$\operatorname{div}_{\text{cyl}}(\boldsymbol{u}) := \operatorname{div}_{(r,z)}\boldsymbol{u} + \frac{u_r}{r} = 0 \qquad \text{where } \operatorname{div}_{(r,z)} := \frac{\partial u_r}{\partial r} + \frac{\partial u_z}{\partial z} \tag{1.6}$$

as well as some quantity c such that

$$\operatorname{div}_{\text{cyl}}(\boldsymbol{j}) = -D\Delta_{\text{cyl}}c + \boldsymbol{u}\cdot\nabla_{(r,z)}c = s \quad \text{where} \quad \boldsymbol{j} := -D\nabla_{(r,z)}c + \boldsymbol{u}c \tag{1.7}$$

where $\nabla_{(r,z)} := (\partial_r c, \partial_z c)^T$ is the gradient with respect to cylindrical coordinates. In [BDM99] an introduction to the proper functional analytical setting for the weak solutions in weighted Sobolev spaces is provided. For the transport equation at hand, it is stated that a weak solution $\widehat{c} \in H^1(\widehat{\Omega})$ of (1.3) corresponds to a weak solution $c \in H^1_1(\Omega)$ of (1.7) where norms are weighted with r.

The dimension reduction has several obvious advantages as it allows for a much simpler geometry description, avoidance of geometry errors and much faster and less costly simulations of the modeled processes compared to full 3D simulations. Besides the computational costs, another important aspect of numerical simulations is physical consistency. In the model at hand, one very important property is that the solution $\widehat{c}$ adheres to the physical bounds posed by min/max principles. That, however, is strongly connected to the divergence constraint on $\widehat{\boldsymbol{u}}$ or $\boldsymbol{u}$. Any violation of $\operatorname{div}(\widehat{\boldsymbol{u}}) = 0$ or $\operatorname{div}_{\text{cyl}}(\boldsymbol{u}) = 0$, respectively, can lead to unphysical over- or undershoots and less accurate approximations of c and its mass fluxes.

DOI 10.20347/WIAS.PREPRINT.3264 Berlin 2026

Therefore, our focus here is on the physically consistent discretization of both equations in their axisymmetric formulation such that mass conservation and min/max principles are preserved exactly. The approach from [FLL11a] for the full three-dimensional problem in Cartesian coordinates relies on a divergence-free Scott–Vogelius finite element method for the Stokes equation and a conservative finite volume method to ensure that the min/max principle also holds for the discrete solution. The approach does not require the same underlying mesh for the transport equation and the Stokes equation and the technical details and aspects for the implementation are discussed in [FLL11a, Sec. 5]. Instead of the rather costly Scott–Vogelius finite element method for the flow, a simple divergence-free postprocessing of some less costly method is also possible as suggested in [Mer+16]. Another relevant approach in this context is [CCG08] where a postprocessed Taylor–Hood method on a triangulation was used for the flow in combination with a Donald box finite volume method for the density in a time-dependent setting.

The present paper transfers the strategy from [FLL11a; Mer+16] to the axisymmetric formulation and provides a proper numerical analysis in weighted Sobolev norms. While the analysis of finite volume methods for transport equations [EGH00; Eym+07; GHV00] and mixed finite element methods for incompressible flow problems [Joh+17; BBF13; Bra07; GR86] is well understood in the Cartesian setting, the axisymmetric case requires weighted Sobolev spaces and a more challenging numerical analysis [BDM99; Rua03; BBD06; LL11; LL12; EJ13; Liu+25].

An investigation of the finite volume scheme for the axisymmetric transport equations and its error analysis in weighted Sobolev norms, which despite its utilization in e.g. [Phi03; KP05; GH05] has not been discussed in detail up to the knowledge of the authors, and therefore is the topic of the first part of the present paper. In particular, linear convergence for the solution $c \in H^2_1(\Omega)$ in a suitable discrete H^1_1 and the L^2_1 norm is shown. In the convective fluxes of the finite volume schemes, the flow field is involved via the quantities $\int_\sigma r\boldsymbol{u} \cdot \boldsymbol{n}\,\mathrm{d}S$ on the boundary segments σ of the control volumes and their sum (according to the divergence theorem) adds up to zero due to $\mathrm{div}_{(r,z)}(r\boldsymbol{u}) = 0$. This divergence constraint for $r\boldsymbol{u}$ is essentially equivalent to mass conservation, as it ensures that no mass is lost or generated within the control volumes of the finite volume method.

When $\boldsymbol{u}$ is replaced by some discrete approximation $\boldsymbol{u}_h$, mass conservation and the validity of the min/max principle hinges on the satisfaction of $\mathrm{div}_{(r,z)}(r\boldsymbol{u}_h) = 0$, which is not straightforward to realize. In fact, even divergence-free methods for the Cartesian setting, like the Scott–Vogelius finite element method employed in [FLL11a], in general do not produce a divergence-free field $r\boldsymbol{u}_h$ in the axisymmetric setting and therefore ultimately may compromise the min/max principles for the discrete quantity c_h. An alternative, where instead $r\boldsymbol{u}$ is approximated directly, is given in [BFO96; Liu+25] on structured rectangular grids.

In order to ensure mass conservation with more flexibility in the choice of the finite element approximations, the present paper suggests to repair the field $r\boldsymbol{u}_h$ by an $H(\mathrm{div},\Omega)$-conforming postprocessing operator Π, similar to what has been done for a $\widehat{\boldsymbol{u}}_h$ that is obtained from a not exactly divergence-free method in the Cartesian setting in [Mer+16]. This results in some auxiliary $H(\mathrm{div},\Omega)$-conforming divergence-free field $\Pi(r\boldsymbol{u}_h)$ and by using $\int_\sigma \Pi(r\boldsymbol{u}_h) \cdot \boldsymbol{n}\ \mathrm{d}S$ for the convective fluxes in the finite volume coupling, the satisfaction of the min/max principles is ensured also in the axisymmetric setting. As in [Mer+16], a lowest-order Bernardi–Raugel finite element method [BR85] is sufficient for the discretization of the axisymmetric Stokes problem. Since we were not able to find results on the well-posedness of the discrete Stokes problem for this method in the literature, we also include a verification of the inf-sup condition establishing well-posedness based on similar results for other popular finite element methods [LL11; LL12; EJ13].

The remaining part of the paper is structured as follows. Section 2 covers some preliminaries, in particular the precise assumptions for the axisymmetry, the resulting weak formulations of the model problems in cylindrical coordinates and the proper function spaces for their analysis. Section 3 explains the finite volume discretization of the transport equation in cylindrical coordinates, including ways to discretize the convective

fluxes such that discrete min/max principles hold. Section 4 is devoted to an a priori error analysis of the finite volume scheme in weighted Sobolev norms. Section 5 discusses the extension to mixed boundary conditions. Section 6 suggest a divergence-free postprocessing for a certain family of finite element methods and includes a proof of the inf-sup stability of the lowest order Bernardi–Raugel finite element method in the axisymmetric setting. Section 7 demonstrates the conservation and convergence properties of the coupled methods in several numerical examples.

2. Preliminaries

This section introduces the full three-dimensional model problem and the axisymmetry condition that allows to apply cylindrical coordinates for a dimension reduction to a two-dimensional problem as well as some notation for weighted Sobolev spaces.

2.1. **The three-dimensional model problem.** In a given three-dimensional domain $\widehat{\Omega}$, we consider the mass transport of a dissolved species in a fluidic medium with mass fraction $\widehat{c}$ according to the convection-diffusion system

$$\operatorname{div}_x(\widehat{\boldsymbol{j}}) = \widehat{s} \quad \text{where} \quad \widehat{\boldsymbol{j}} := -D\nabla_x \widehat{c} + \widehat{\boldsymbol{u}}\,\widehat{c}. \tag{2.1}$$

Here, $\widehat{s}$ is a given volume source term and $\widehat{\boldsymbol{u}} : \widehat{\Omega} \to \mathbb{R}^3$ is the velocity field of the fluid, which may be given as an analytic function or as an approximation from a finite element method. The subscript x for the differential operators indicates that they are evaluated with respect to Cartesian coordinates.

The velocity field $\widehat{\boldsymbol{u}}$, together with some pressure $\widehat{p}$, solves the incompressible Stokes equations

$$-\nu\Delta_x \widehat{\boldsymbol{u}} + \nabla_x \widehat{p} = \widehat{\boldsymbol{f}} \quad \text{and} \quad \operatorname{div}_x \widehat{\boldsymbol{u}} = 0 \tag{2.2}$$

for a given volume force $\widehat{\boldsymbol{f}}$.

Boundary conditions for both subproblems are specified later after the introduction of the respective axisymmetric problems and the necessary notation.

2.2. **Axisymmetry and weighted Sobolev spaces.** In this paper, we are interested in an axisymmetric setting and assume that the three-dimensional computational domain $\widehat{\Omega}$ is obtained by rotation of a two-dimensional polygonal cross-section domain $\Omega \subset \mathbb{R}^+ \times \mathbb{R}$, i.e., $\widehat{\Omega} := \{\boldsymbol{x} = \Phi(r,\theta,z) : (r,z) \in \Omega,\ \theta \in [0,2\pi)\}$. Here, (r,θ,z) denote cylindrical coordinates defined by $\Phi :\ (r,\theta,z) \mapsto (r\cos(\theta), r\sin(\theta), z)^T$, where r and z is the distance to the axis of revolution and the height, respectively. Given the axis of revolution $\Gamma_{\mathrm{rot}} := \{(r,z) \in \overline{\Omega} : r = 0\}$, we denote by $\Gamma := \overline{(\partial\Omega \setminus \Gamma_{\mathrm{rot}})}^{\partial\Omega}$ the closure of the points on the boundary outside of Γ_{rot}. This in particular includes the corners shared by Γ_{rot} and Γ where different kinds of boundary conditions may meet.

We call a scalar function $\widehat{v} : \widehat{\Omega} \to \mathbb{R}$ axisymmetric if it is invariant with respect to θ. Then $v(\Phi(r,\theta,z)) := \widehat{v}(r,z)$ for any $\theta \in [0,2\pi[$ is its transformed counterpart on Ω. Note, that the axisymmetry of $\widehat{v}$ implies homogeneous Neumann boundary conditions for v along Γ_{rot}.

The analysis of the axisymmetric problems involves weighted Sobolev spaces

$$\begin{aligned} L^2_s(\Omega) &:= \left\{ v : \|v\|^2_{L^2_s(\Omega)} < \infty \right\}, \\ H^m_s(\Omega) &:= \left\{ v : \partial^\alpha v \in L^2_s(\Omega) \text{ for all } \alpha \in \mathbb{N}^2 \text{ with } |\alpha| \le m \right\} \end{aligned}$$

with the partial derivatives $\partial^\alpha := \partial_r^{\alpha_1}\partial_z^{\alpha_2}$, $\partial^{(0,0)}v := v$ and norms

$$\|v\|^2_{L^2_s(\Omega)} := \int_\Omega v^2 r^s \,\mathrm{d}r\,\mathrm{d}z, \quad \text{and} \quad \|v\|^2_{H^m_s(\Omega)} := \sum_{\substack{\alpha\in\mathbb{N}^2,\\ |\alpha|\le m}} \|\partial^\alpha v\|^2_{L^2_s(\Omega)}.$$

The proper trace space on some part $\gamma \subseteq \Gamma$ of the boundary reads

$$H_1^{1/2}(\gamma) := \left\{ g \in L_1^2(\gamma) : \exists v \in H_1^1(\Omega), v|_\gamma = g \right\}.$$

The trace operator $v \mapsto v|_\gamma$ is continuous from $H_1^1(\Omega)$ to $H_1^{1/2}(\gamma)$. Details can be found in [BDM99] together with some well-posedness and regularity results for certain model problems in axisymmetric formulation, in particular the Laplace problem and the Stokes problem.

2.3. **Transformation of the transport equation.** Under homogeneous Neumann boundary conditions on Γ_{rot} (due to axisymmetry) and Dirichlet boundary conditions on the remaining boundary Γ, i.e. $c = g$ for some $g \in H_1^{1/2}(\Gamma)$, one looks for solutions $c \in g + H^1_{1,0}(\Omega)$ where

$$H^1_{1,0}(\Omega) := \left\{ v \in H_1^1(\Omega) \ : \ v|_\Gamma = 0 \right\}.$$

The variational formulation of (2.1) follows from testing with some $\phi \in H^1_{1,0}(\Omega)$ and transforming the integrals to cylindrical coordinates, i.e.,

$$\begin{aligned} 2\pi \int_\Omega rs\,\phi \,\mathrm{d}r\,\mathrm{d}z = \int_{\widehat\Omega} \widehat{s}\,\widehat{\phi}\,\mathrm{d}x &= \int_{\widehat\Omega} D\nabla_x \widehat{c}\cdot\nabla_x\widehat{\phi} + \widehat{\boldsymbol{u}}\nabla_x\widehat{c}\,\widehat{\phi}\,\mathrm{d}x \\ &= 2\pi\int_\Omega r\left[D\nabla_{(r,z)}c\cdot\nabla_{(r,z)}\phi + \boldsymbol{u}\cdot\nabla_{(r,z)}c\,\phi\right]\mathrm{d}r\,\mathrm{d}z. \end{aligned}$$

Neglecting the factor 2π leaves us with the weak axisymmetric formulation of the transport equation: seek $c \in g + H^1_{1,0}(\Omega)$, such that, for all $\phi \in H^1_{1,0}(\Omega)$,

$$\int_\Omega \left[D\nabla c\cdot\nabla\phi + \boldsymbol{u}\cdot\nabla c\,\phi\right] r \,\mathrm{d}r\,\mathrm{d}z =: A(c,\phi) = s(\phi) := \int_\Omega s\,\phi\, r\,\mathrm{d}r\,\mathrm{d}z. \tag{2.3}$$

2.4. **Transformation of the Stokes problem.** A three-dimensional vector field $\widehat{\boldsymbol{v}} : \widehat\Omega \to \mathbb{R}^3$ is said to be axisymmetric, if its three components are axisymmetric, i.e., there exist $v_r : \Omega \to \mathbb{R}$, $v_z : \Omega \to \mathbb{R}$ and $v_\theta : \Omega \to \mathbb{R}$ such that

$$\begin{aligned} \widehat{\boldsymbol{v}}(\Phi(r,\theta,z)) &= v_r(r,z)\boldsymbol{e}_r(\theta) + v_\theta(r,z)\boldsymbol{e}_\theta(\theta) + v_z(r,z)\boldsymbol{e}_z \\ &= (v_r(r,z)\cos\theta - v_\theta(r,z)\sin\theta)\boldsymbol{e}_x \\ &\quad + (v_r(r,z)\sin\theta + v_\theta(r,z)\cos\theta)\boldsymbol{e}_y + v_z(r,z)\boldsymbol{e}_z \end{aligned}$$

where $\boldsymbol{e}_r(\theta) := \cos\theta\boldsymbol{e}_x + \sin\theta\boldsymbol{e}_y$ and $\boldsymbol{e}_\theta(\theta) := -\sin\theta\boldsymbol{e}_x + \cos\theta\boldsymbol{e}_y$ are the (angle-dependent) unit vectors in the r- and θ-directions.

Under the assumption that the data $\boldsymbol{f} = (f_r(r,z), f_z(r,z))$ is axisymmetric and has a vanishing angular component, i.e. $f_\theta \equiv 0$, the Stokes problem has a unique axisymmetric solution $\boldsymbol{u}$ with a vanishing angular component $u_\theta = 0$ [BDM99, Sec. IX.1].

This solution can be characterized by the axisymmetric formulation of the Stokes problem, see e.g. [BDM99, Eq. (I.3.11)], which seeks a velocity $\boldsymbol{u} = u_\Gamma + (u_z, u_r) \in u_\Gamma + \mathbf{V}$ and a pressure $p \in Q$ in spaces defined

below, such that

$$\begin{aligned} -\nu\left(\Delta_{\text{cyl}} u_r - \frac{u_r}{r^2}\right) + \frac{\partial p}{\partial r} &= f_r, \\ -\nu\Delta_{\text{cyl}} u_z + \frac{\partial p}{\partial z} &= f_z, \\ \operatorname{div}_{\text{cyl}}(\boldsymbol{u}) = \operatorname{div}_{(r,z)}\boldsymbol{u} + \frac{u_r}{r} &= 0 \end{aligned}$$

where u_Γ denotes the inhomogeneous Dirichlet boundary conditions along Γ. The weak formulation involves the weighted Sobolev spaces

$$\begin{aligned} H^1_-(\Omega) &:= \left\{v \in H^1_1(\Omega) \cap L^2_{-1}(\Omega) : v|_{\Gamma_{\text{rot}}} = 0\right\}, \\ H^1_+(\Omega) &:= \left\{v \in H^1_1(\Omega) : \partial_r v|_{\Gamma_{\text{rot}}} = 0\right\} \end{aligned}$$

for the velocity components in the r- and z-directions, where $H^1_-(\Omega)$ incorporates the condition $\boldsymbol{u}\cdot\boldsymbol{n} = u_r = 0$ at the axis of revolution. The two spaces form the product space $\mathbf{V} := H^1_-(\Omega)\times H^1_+(\Omega)$ with the product and energy norm

$$|||\boldsymbol{v}|||^2 := \|v_r\|^2_{H^1_1(\Omega)} + \|v_r\|^2_{L^2_{-1}(\Omega)} + \|v_z\|^2_{H^1_1(\Omega)}.$$

The pressure is sought in the space

$$Q := L^2_{1,0} := \left\{q \in L^2_1(\Omega) : \int_\Omega qr\,\mathrm{d}r\,\mathrm{d}z = 0\right\}.$$

Then, the weak solution $(\boldsymbol{u}, p) \in (u_\Gamma + \mathbf{V})\times Q$ is characterized by

$$a(\boldsymbol{u},\boldsymbol{v}) + b(p,\boldsymbol{v}) = (\boldsymbol{f}, r\boldsymbol{v})_{L^2} \qquad \text{for all } \boldsymbol{v}\in V, \tag{2.4}$$

$$b(q,\boldsymbol{u}) = 0 \qquad \text{for all } q \in Q, \tag{2.5}$$

where the bilinear forms stem from the transformation of the corresponding three-dimensional bilinear forms, i.e.,

$$\begin{aligned} a(\boldsymbol{u},\boldsymbol{v}) &:= \int_\Omega \left(\nabla_{(r,z)}\boldsymbol{u} : \nabla_{(r,z)}\boldsymbol{v} + r^{-2}u_r v_r\right) r\,\mathrm{d}r\,\mathrm{d}z = \frac{1}{2\pi}\int_{\widehat{\Omega}} \nabla_x\widehat{\boldsymbol{u}} : \nabla_x\widehat{\boldsymbol{v}}\,\mathrm{d}x, \\ b(q,\boldsymbol{v}) &:= -\int_{\widehat{\Omega}} q\operatorname{div}_{(r,z)}(r\boldsymbol{v})\,\mathrm{d}r\,\mathrm{d}z = -\int_\Omega q\left(\operatorname{div}(\boldsymbol{v}) + r^{-1}v_r\right) r\,\mathrm{d}r\,\mathrm{d}z \\ &= -\frac{1}{2\pi}\int_{\widehat{\Omega}} \widehat{q}\operatorname{div}_x\widehat{\boldsymbol{v}}\,\mathrm{d}x. \end{aligned}$$

Remark 2.1. In case the data $\boldsymbol{f}$ has an angular component, i.e. $f_\theta \neq 0$, an additional (uncoupled) azimuthal equation has to be solved to determine the angular component u_θ of the solution, see e.g. [BDM99, Sec. IX.1.8]. Throughout this paper we assume $f_\theta = 0$ and therefore $u_\theta = 0$ for simplicity.

3. Finite volume discretization of the axisymmetric transport equation

This section describes the discretization of the transport equation in the axisymmetric formulation by a two-point flux finite volume method.

3.1. **Admissible meshes and notation.** Let $\mathcal{T}$ be a boundary-conforming Delaunay triangulation of Ω with vertices $\mathcal{N}$, corresponding Voronoi cells $\mathcal{K}$ and their edges $\mathcal{E}$. Then $(\mathcal{K}, \mathcal{E}, \mathcal{N})$ is a restricted admissible mesh in the sense of [GHV00, Def. 2.1], see Figure 3.1 for an example.

We denote for any $\omega \subseteq \overline{\Omega}$ by $\mathcal{E}(\omega) := \{\sigma \in \mathcal{E} : \sigma \subset \overline{\omega}\}$ the set of edges within ω. The set $\mathcal{N}(\omega)$ and $\mathcal{K}(\omega)$ denotes the set of vertices within ω and the set of control volumes with incident edges $\sigma \subset \omega$, respectively. We also denote by $\mathcal{E}_{\rm int} := \mathcal{E} \setminus \mathcal{E}(\partial\Omega)$ the set of all interior edges that do not lie on the boundary $\partial\Omega$. For any distinct $K, L \in \mathcal{K}$, their associated vertices x_k and x_L, and their shared interior edge $K|L = \sigma \in \mathcal{E}$ we write $d_{K,\sigma}$ for the Euclidean distance between x_K and σ and $d_\sigma := 2d_{K,\sigma} = 2d_{L,\sigma}$. Since all vertices $x_K \in \mathcal{N}$ for boundary cells $K \in \mathcal{K}$ are contained on boundary edges $\sigma \subset \partial\Omega$, we set $d_\sigma = 0$ for $\sigma \in \mathcal{E}(\partial\Omega)$.

For any edge $\sigma \in \mathcal{E}$, we denote the length of σ by $|\sigma|$ and write $\mathrm{mid}(\sigma)$ for the mid-point of σ. The neighbouring control volumes of $K \in \mathcal{K}$ are denoted by $\mathcal{K}_{\rm N}(K) := \mathcal{K}(\overline{K}) \setminus \{K\}$ and the maximal mesh width is denoted by $\mathrm{size}(\mathcal{K}) := \max_{K\in\mathcal{K}} \mathrm{diam}(K)$. Moreover, $P_0(\mathcal{K})$ denotes the set of piecewise constant functions with respect to $\mathcal{K}$.

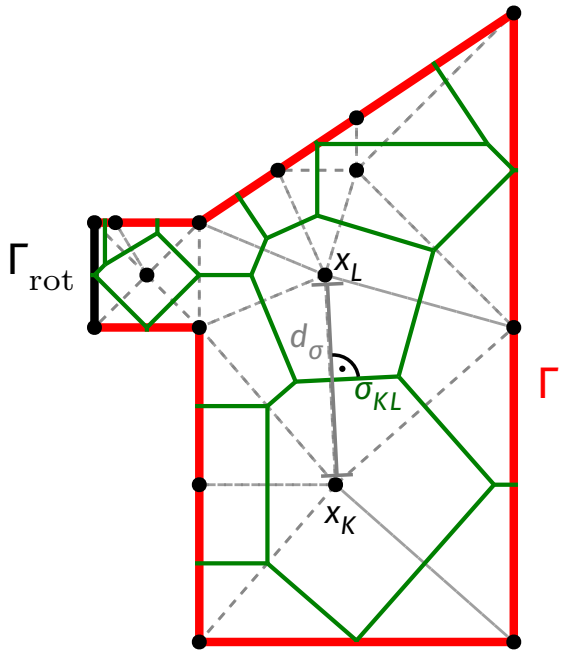

FIGURE 3.1. Sketch of key components of an admissible mesh for a polygonal domain $\Omega \subset \mathbb{R}^2$.

3.2. **The discrete scheme.** The finite volume method seeks a piecewise constant function $c_h = (c_K)_{K\in\mathcal{K}} \in P_0(\mathcal{K})$ which satisfies

$$\sum_{\sigma\in\mathcal{E}(K)} (F_{K,\sigma} + V_{K,\sigma}) = s_K \quad \text{for all } K \in \mathcal{K} \setminus \mathcal{K}(\Gamma) \quad \text{where} \quad s_K := \int_K r\, s\, \mathrm{d}r\, \mathrm{d}z. \tag{3.1}$$

For the Dirichlet boundary volumes $K \in \mathcal{K}(\Gamma)$ with vertices $x_K \in \mathcal{N}(\Gamma)$, the unknowns c_K are set according to

$$c_K = J\left(g|_\sigma\right) \quad \text{for } \sigma \in \mathcal{E}(K) \cap \mathcal{E}(\Gamma), \tag{3.2}$$

where J is a suitable functional for the evaluation of the boundary condition discussed in Remark 3.1 below.

The flux $F_{K,\sigma}$ in (3.1) is defined by

$$F_{K,\sigma} := -\tau_\sigma\left(c_L - c_K\right) \quad \text{with} \quad \tau_\sigma := \begin{cases} |\sigma| r(\mathrm{mid}(\sigma))/d_\sigma & \text{if } \sigma = K|L, \\ 0 & \text{else} \end{cases} \tag{3.3}$$

and approximates the diffusive flux $\int_\sigma r D \nabla c \cdot \boldsymbol{n}_{K,\sigma}\,\mathrm{d}S$ across $\sigma \in \mathcal{E}$. The quantity $V_{K,\sigma} := u_{K,\sigma} c_{\sigma,+}$ in (3.1) approximates the convective flux $\int_\sigma r c\,\boldsymbol{u} \cdot \boldsymbol{n}_{K,\sigma}\,\mathrm{d}S$. For the latter, we choose an unconditionally stable upwinding flux discretization where

$$u_{K,\sigma} := \int_\sigma r\,\boldsymbol{u} \cdot \boldsymbol{n}_{K,\sigma}\,\mathrm{d}S \tag{3.4}$$

determines the upwind direction such that

$$\text{if } \sigma = K|L, \quad c_{\sigma,+} := \begin{cases} c_K & \text{if } u_{K,\sigma} \geq 0, \\ c_L & \text{else,} \end{cases} \tag{3.5}$$

$$\text{if } \sigma \in \mathcal{E}(\partial\Omega) \cap \mathcal{E}(K), \quad c_{\sigma,+} := c_K. \tag{3.6}$$

Note that we can rewrite (3.1) as

$$s_K = \sum_{\substack{\sigma = K|L \\ L \in \mathcal{K}_{\mathrm{N}}(K)}} \tau_{KL}\left(1 + \frac{|u_{K,\sigma}|}{2\tau_{KL}}\right)\left(c_K - c_L\right) + \tau_{KL}\frac{u_{K,\sigma}}{2\tau_{KL}}\left(c_K + c_L\right). \tag{3.7}$$

Subsequently, also the *downstream* value of c_h plays a role and reads

$$c_{\sigma,-} := \begin{cases} c_L & \text{if } u_{K,\sigma} \geq 0, \\ c_K & \text{else.} \end{cases}$$

Remark 3.1 (choice of J)**.** If g is sufficiently smooth (such as in the case $g \in H_1^{3/2}(\Gamma)$ where g is also continuous), we set $J(g|_\sigma) := g(x_K)$ for the volume K with $\sigma \in \mathcal{E}(K)$ and collocation point $x_K \in \Gamma$. Otherwise, one can use the integral average $J(g|_\sigma) := (r(\mathrm{mid}(\sigma))|\sigma|)^{-1} \int_\sigma r\,g\,\mathrm{d}S$.

Remark 3.2 (toroidal control volumes)**.** The main difference to a finite volume method in Cartesian coordinates is the factor $r(\mathrm{mid}(\sigma))$ in the transmission coefficients, which links the control volumes of the two-dimensional control volumes in Ω with the toroidal volumes of the control volumes in $\widehat{\Omega}$ that one obtains by rotation (up to the factor 2^π). From an analytical point of view one then has the choice to study the convergence with polygonal control volumes in weighted norms or with the usual norms in toroidal control volumes. The analysis in the present paper follows the first possibility.

3.3. **Discrete min/max principle.** The following classical min/max principle holds.

Theorem 3.3. For any solution $(c_K)_{K \in \mathcal{K}}$ of (3.1) – (3.2) and convective fluxes $u_{K,\sigma}$ that are divergence free in the finite volume sense

$$\sum_{\substack{\sigma = K|L \\ L \in \mathcal{K}_{\mathrm{N}}(K)}} u_{K,\sigma} = 0 \quad \forall K \in \mathcal{K} \setminus \mathcal{K}(\Gamma) \tag{3.8}$$

the following conditions hold:

(i) *Local min/max principle:*

(3.9) If $s_K \leq 0$, then $c_K \leq \max_{L\in\mathcal{K}_\mathrm{N}(K)} c_L \quad \forall K \in \mathcal{K}\setminus\mathcal{K}(\Gamma)$,

(3.10) If $s_K \geq 0$, then $c_K \geq \min_{L\in\mathcal{K}_\mathrm{N}(K)} c_L \quad \forall K \in \mathcal{K}\setminus\mathcal{K}(\Gamma)$.

(ii) *Global min/max principle:* If $s_K \leq 0$ (resp. $s_K \geq 0$) for all $K \in \mathcal{K}\setminus\mathcal{K}(\Gamma)$, then the solution $(c_K)_{K\in\mathcal{K}}$ assumes its maximum (resp. minimum) on the Dirichlet boundary Γ and furthermore, it holds that

(3.11) If $s_K \leq 0$ for all $K \in \mathcal{K}$, then $c_K \leq \max_{L\in\mathcal{K}(\Gamma)} c_L \quad \forall K \in \mathcal{K}$,

(3.12) If $s_K \geq 0$ for all $K \in \mathcal{K}$, then $c_K \geq \min_{L\in\mathcal{K}(\Gamma)} c_L \quad \forall K \in \mathcal{K}$.

Proof of (i). The proof does not differ significantly from the proof in, e.g., [FLL11a, Lemma 4.4] for the Cartesian setting, but is included here for completeness and to stress the role of (3.8).

Due to (3.7), we have for all $K \in \mathcal{K}\setminus\mathcal{K}(\Gamma)$:

$$s_K = c_K \sum_{\substack{\sigma=K|L\\ L\in\mathcal{K}_\mathrm{N}(K)}} \tau_{KL}\left(1+\frac{|u_{K,\sigma}|}{2\tau_{KL}}+\frac{u_{K,\sigma}}{2\tau_{KL}}\right) + \sum_{\substack{\sigma=K|L\\ L\in\mathcal{K}_\mathrm{N}(K)}} \tau_{KL}\left(-1-\frac{|u_{K,\sigma}|}{2\tau_{KL}}+\frac{u_{K,\sigma}}{2\tau_{KL}}\right) c_L$$

$$=: c_K\eta_K + \sum_{\substack{\sigma=K|L\\ L\in\mathcal{K}_\mathrm{N}(K)}} \sigma_{KL}c_L, \tag{3.13}$$

where $\eta_K > 0$ and $\sigma_{KL} < 0$. Furthermore, we have

$$\begin{aligned} -\sum_{\substack{\sigma=K|L\\ L\in\mathcal{K}_\mathrm{N}(K)}} \sigma_{KL} &= \sum_{\substack{\sigma=K|L\\ L\in\mathcal{K}_\mathrm{N}(K)}} \tau_{KL}\left(1+\frac{|u_{K,\sigma}|}{2\tau_{KL}}-\frac{u_{K,\sigma}}{2\tau_{KL}}\right)\\ &= \sum_{\substack{\sigma=K|L\\ L\in\mathcal{K}_\mathrm{N}(K)}} \tau_{KL}\left(1+\frac{|u_{K,\sigma}|}{2\tau_{KL}}+\frac{u_{K,\sigma}}{2\tau_{KL}}\right) - \sum_{\substack{\sigma=K|L\\ L\in\mathcal{K}_\mathrm{N}(K)}} u_{K,\sigma} = \eta_K \end{aligned} \tag{3.14}$$

where in the last step, we exploited (3.8). If $s_K \leq 0$, (3.13) yields

$$c_K \leq \sum_{\substack{\sigma=K|L\\ L\in\mathcal{K}_\mathrm{N}(K)}} -\frac{\sigma_{KL}}{\eta_K}c_L \leq \max_{L\in\mathcal{K}_\mathrm{N}(K)} c_L \underbrace{\sum_{\substack{\sigma=K|L\\ L\in\mathcal{K}_\mathrm{N}(K)}} -\frac{\sigma_{KL}}{\eta_K}}_{\overset{(3.14)}{=}1} = \max_{L\in\mathcal{K}_\mathrm{N}(K)} c_L$$

and thus (3.9) follows. A similar argument can be used to show (3.10). □

Proof of (ii). For the proof of (3.11) let $c^* := \max_{K\in\mathcal{K}} c_K$ and assume $c^* = c_{K^*}$ for some $K^* \in \mathcal{K}\setminus\mathcal{K}(\Gamma)$. Then, (i) shows

$$c^* = c_{K^*} \leq \sum_{\substack{\sigma=K|L\\ L\in\mathcal{K}_\mathrm{N}(K)}} -\frac{\sigma_{KL}}{\eta_K}c_L \leq \max_{L\in\mathcal{K}_\mathrm{N}(K)} c_L \leq c^*.$$

Due to (3.14), this implies that $c_L = c^*$ for all $L \in \mathcal{N}_{K^*}$. The argument can be repeated across all neighbours and since all cells $K \in \mathcal{K}$ can eventually be reached via this process, the solution $(c_K)_{K\in\mathcal{K}}$ is constant and must equal c^* everywhere, which then is also the value on the boundary. The estimate (3.12) can be proven similarly by starting with $c_* := \min_{K\in\mathcal{K}} c_K$. □

Remark 3.4 (mass conservation)**.** The proof of the maximum principle requires (3.8). If $\widehat{\boldsymbol{u}}$ is a given divergence-free vector field, this follows via

$$\sum_{\substack{\sigma=K|L\\ L\in\mathcal{K}_{\mathrm{N}}(K)}} u_{K,\sigma} = \int_{\partial K} r\,\boldsymbol{u}\cdot\boldsymbol{n}_{K,\sigma}\,\mathrm{d}S = \int_K \mathrm{div}_{(r,z)}(r\boldsymbol{u})\,\mathrm{d}r\,\mathrm{d}z = \frac{1}{2\pi}\int_{\widehat{K}} \mathrm{div}_x(\widehat{\boldsymbol{u}})\,\mathrm{d}x = 0.$$

If $\widehat{\boldsymbol{u}}$ or $\boldsymbol{u}$ is approximated by a numerical method, the mass conservation may be compromised if the divergence constraint is not met exactly or if the integrals $u_{K,\sigma}$ are not computed with sufficient accuracy.

Remark 3.5 (uniqueness of discrete solution)**.** It is well known that Theorem 3.3 also implies unique solvability. Indeed, the min/max principle shows that the linear solution operator associated with (3.1) – (3.2) is injective and therefore also surjective due to the rank-nullity theorem.

4. A PRIORI ERROR ANALYSIS OF THE FVM

Our error analysis follows that in [GHV00] for the Cartesian setting and relies on extracting error estimates for the approximate finite volume solution of (3.1). The main differences concern a weighted discrete energy norm and an appropriate discrete Poincaré inequality.

4.1. Discrete energy norm and Poincaré inequality.

The analysis involves the discrete space

$$W_{h,0}(\mathcal{K}) := \Big\{c_h \in P_0(\mathcal{K}) : c_h|_K = 0 \quad \text{for } K \in \mathcal{K}(\Gamma)\Big\}. \tag{4.1}$$

and the discrete norm on $W_h(\mathcal{K})$ defined by

$$\|c_h\|_{1,\mathcal{K}} := \left(\sum_{\sigma\in\mathcal{E}_{\mathrm{int}}} \tau_\sigma (D_\sigma c_h)^2\right)^{1/2} \quad \text{with} \quad D_\sigma := c_K - c_L \text{ for } \sigma = K|L \in \mathcal{E}_{\mathrm{int}}. \tag{4.2}$$

Recall that the factors τ_σ according to (3.3) include the radius such that this norm can be seen as a discrete $H^1_{1,0}(\Omega)$ norm. For the piecewise constant functions $P_0(\mathcal{K})$ it is only a semi norm. Here and throughout, the discrete trace $\gamma c_h : \partial\Omega \to \mathbb{R}$ of some $c_h \in P_0(\mathcal{K})$ is defined by $\gamma c_h := c_K$ a.e. on $\sigma \in \mathcal{E}(K)\cap\mathcal{E}(\partial\Omega)$.

For the stability and error estimates, the following discrete Poincaré inequality is required.

Lemma 4.1 (Discrete Poincaré Inequality)**.** For any $c_h \in P_0(\mathcal{K})$, there holds

$$\|c_h\|_{L^2_1(\Omega)} \lesssim \|c_h\|_{1,\mathcal{K}} + \|\gamma c_h\|_{L^2_1(\Gamma)}. \tag{4.3}$$

with a constant that only depends on $\mathrm{diam}(\Omega)$. For $c_h \in W_{h,0}(\mathcal{K})$, the second term on the right-hand side vanishes.

Proof of Lemma 4.1. Let $\boldsymbol{d} := [0,1]^T$ (or alternatively $\boldsymbol{d} := [0,-1]^T$) the second canonical unit vector in $\mathbb{R}^2$. Given $K \in \mathcal{K}$ and $x \in K$, we choose $y(x) := x + s\boldsymbol{d} \in \Gamma$ with minimal $s > 0$. We also write for any two points $x, y \in \Omega$ the line segment joining x and y as $[x,y] := \{(1-t)x + ty \,|\, t \in [0,1]\}$.

Let us now define for $\sigma = K|L \in \mathcal{E}_{\mathrm{int}}$ the function $\chi_\sigma : \mathbb{R}^2 \to \{0,1\}$ by

$$\chi_\sigma(x) := \begin{cases} 1 & \text{if } \sigma \cap [x, y(x)] \neq \emptyset, \\ 0 & \text{else.} \end{cases}$$

The function χ_σ is the characteristic function of the "shadow" of σ in the opposite direction of $\boldsymbol{d}$, see Figure 4.1.

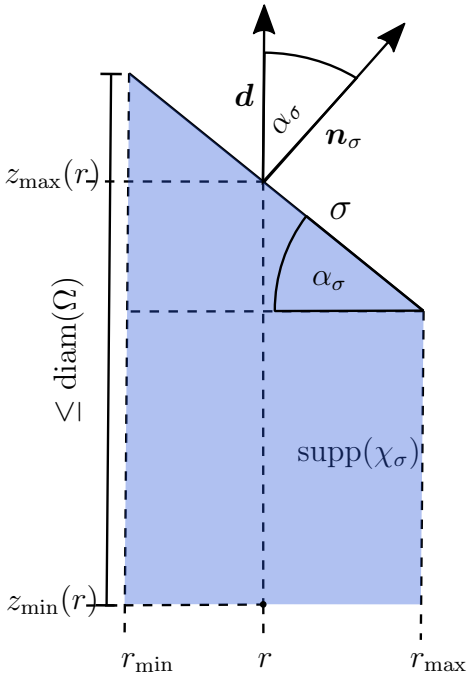

FIGURE 4.1. Illustration of the parametrization of $\operatorname{supp}(\chi_\sigma)$. Note that $r_{\max} - r_{\min} = |\sigma| \cos(\alpha_\sigma) = |\sigma||\boldsymbol{d} \cdot \boldsymbol{n}_\sigma| = |\sigma| c_\sigma$.

For almost every $x \in K$ (up to finitely many occasions where an edge σ or a vertex of the mesh is included in $[x, y(x)]$) a series of triangle inequalities yields

$$|c_h(x)| = |c_K| \leq \sum_{\sigma \in \mathcal{E}_{\mathrm{int}}} D_\sigma c_h \, \chi_\sigma(x) + \sum_{\sigma \in \mathcal{E}(\Gamma)} c_h(x_\sigma) \chi_\sigma(x) =: A(x) + B(x), \tag{4.4}$$

where we denote by $x_\sigma \in \mathcal{N}(\Gamma)$ the collocation point of the boundary volume $M \in \mathcal{K}(\Gamma)$ of which $\sigma \in \mathcal{E}(M) \cap \mathcal{E}(\Gamma)$ is an edge. W.l.o.g. we choose $\boldsymbol{n}_\sigma$ such that $c_\sigma := \boldsymbol{d} \cdot \boldsymbol{n}_\sigma > 0$ (since σ is not included in $[x, y(x)]$), square and apply a Cauchy inequality to obtain

$$\begin{aligned} A(x)^2 &\leq \left(\sum_{\sigma \in \mathcal{E}_{\mathrm{int}}} \left(\frac{1}{\sqrt{d_\sigma c_\sigma}} D_\sigma c_h \sqrt{\chi_\sigma(x)} \right) \left(\sqrt{d_\sigma c_\sigma \chi_\sigma(x)} \right) \right)^2 \\ &\leq \left(\sum_{\sigma \in \mathcal{E}_{\mathrm{int}}} \frac{(D_\sigma c_h)^2}{d_\sigma c_\sigma} \chi_\sigma(x) \right) \left(\sum_{\sigma \in \mathcal{E}_{\mathrm{int}}} d_\sigma c_\sigma \chi_\sigma(x) \right). \end{aligned} \tag{4.5}$$

A telescoping series with final collocation point $x_M \in \Gamma$ results in

$$\sum_{\sigma \in \mathcal{E}_{\mathrm{int}}} c_\sigma d_\sigma \chi_\sigma(x) \leq \sum_{\sigma \in \mathcal{E}_{\mathrm{int}}} \boldsymbol{d} \cdot \boldsymbol{n}_\sigma \chi_\sigma(x) \leq \boldsymbol{d} \cdot (x_M - x_K) \leq \operatorname{diam}(\Omega).$$

Similarly, one estimates

$$B(x)^2 \le \left(\sum_{\sigma\in\mathcal{E}(\Gamma)} \left(\frac{1}{\sqrt{c_\sigma}} c_h(x_\sigma)\sqrt{\chi_\sigma(x)} \right) \left(\sqrt{c_\sigma \chi_\sigma(x)} \right) \right)^2$$
$$\le \left(\sum_{\sigma\in\mathcal{E}(\Gamma)} \frac{c_h(x_\sigma)^2}{c_\sigma} \chi_\sigma(x) \right) \left(\sum_{\sigma\in\mathcal{E}(\Gamma)} c_\sigma \chi_\sigma(x) \right) \le \sum_{\sigma\in\mathcal{E}(\Gamma)} \frac{c_h(x_\sigma)^2}{c_\sigma} \chi_\sigma(x).$$

The weighted integral of (4.5) to compute the $L^2_1(\Omega)$ norm of c_h reads

$$\|c_h\|^2_{L^2_1(\Omega)} = \sum_{K\in\mathcal{K}} \int_K r|c_K|^2 \,\mathrm{d}r\,\mathrm{d}z \le \sum_{K\in\mathcal{K}} \int_K r\left(A(x)^2 + B(x)^2\right) \mathrm{d}r\,\mathrm{d}z$$
$$= \left(\operatorname{diam}(\Omega) \sum_{\sigma\in\mathcal{E}_{\mathrm{int}}} \frac{(D_\sigma c_h)^2}{d_\sigma} I_\sigma + \sum_{\sigma\in\mathcal{E}(\Gamma)} c_h(x_\sigma)^2 I_\sigma \right), \tag{4.6}$$
$$\text{where } I_\sigma := \frac{1}{c_\sigma} \int_\Omega r\,\chi_\sigma((r,z))\,\mathrm{d}r\,\mathrm{d}z.$$

The parametrization $\operatorname{supp}(\chi_\sigma(x)) := (r_{\min}(\sigma), r_{\max}(\sigma)) \times (z_{\min}(x), z_{\max}(x))$ of the support of $\chi_\sigma(x)$, recall Figure 4.1, allows to rewrite the remaining integral as

$$c_\sigma I_\sigma = \int_\Omega r\,\chi_\sigma((r,z))\,\mathrm{d}r\,\mathrm{d}z = \int_{r_{\min}}^{r_{\max}} r \int_{z_{\min}(r)}^{z_{\max}(r)} \chi_\sigma((r,z))\,\mathrm{d}z\,\mathrm{d}r \tag{4.7}$$
$$\le \operatorname{diam}(\Omega)\frac{1}{2}\left(r_{\max}^2 - r_{\min}^2\right)$$
$$= \operatorname{diam}(\Omega)\frac{1}{2}(r_{\max} + r_{\min})(r_{\max} - r_{\min})$$
$$= \operatorname{diam}(\Omega) r(\operatorname{mid}(\sigma)) c_\sigma |\sigma|.$$

Inserting $I_\sigma \le \operatorname{diam}(\Omega) r(\operatorname{mid}(\sigma))|\sigma|$ into (4.6) yields

$$\|c_h\|^2_{L^2_1(\Omega)} \le \operatorname{diam}(\Omega)^2 \sum_{\sigma\in\mathcal{E}_{\mathrm{int}}} \frac{(D_\sigma c_h)^2}{d_\sigma} r(\operatorname{mid}(\sigma))|\sigma| + \operatorname{diam}(\Omega) \sum_{\sigma\in\mathcal{E}(\Gamma)} c_h(x_\sigma)^2 r(\operatorname{mid}(\sigma))|\sigma|$$
$$= \operatorname{diam}(\Omega)^2 \|c_h\|^2_{1,\mathcal{K}} + \operatorname{diam}(\Omega)\|c_h\|^2_{L^2_1(\Gamma)}.$$

This concludes the proof. □

Remark 4.2. The critical calculation in (4.7) also holds for $\boldsymbol{d} = [1,0]^T$. Similar to Figure 4.1, now $z_{\min}$ and $z_{\max}$ are fixed and $r_{\max}(z) \in (r_1, r_2)$ denotes the maximal radius in dependence of z, while r_1 and r_2 is

the minimal and maximal radius of σ, respectively. Then, one obtains

$$\begin{aligned} c_\sigma I_\sigma &= \int_\Omega r\,\chi_\sigma((r,z))\,\mathrm{d}r\,\mathrm{d}z \\ &= \int_{z_{\min}}^{z_{\max}} \left(\int_0^{r_1} r\,\chi_\sigma((r,z))\,\mathrm{d}r + \int_{r_1}^{r_{\max(z)}} r\,\chi_\sigma((r,z))\,\mathrm{d}r \right) \mathrm{d}z \\ &= \frac{1}{2} r_1^2 c_\sigma |\sigma| + \int_{z_{\min}}^{z_{\max}} \frac{1}{2}\left(r_{\max}(z) + r_1\right)\left(r_{\max}(z) - r_1\right)\mathrm{d}z \\ &\leq \frac{3}{2}\,\mathrm{diam}(\Omega)\, r(\mathrm{mid}(\sigma))\, c_\sigma |\sigma|. \end{aligned}$$

The following Lemma aids us in establishing a standard stability estimate.

Lemma 4.3. For any $c_h = (c_K)_{K\in\mathcal{K}} \in W_{h,0}(\mathcal{K})$, it holds

$$\sum_{K\in\mathcal{K}} \sum_{\sigma\in\mathcal{E}(K)} F_{K,\sigma} c_K + V_{K,\sigma} c_K \geq \|c_h\|_{1,\mathcal{K}}^2 + \frac{1}{2}\int_\Omega \mathrm{div}_{(r,z)}(r\boldsymbol{u})\, c_h^2\,\mathrm{d}r\,\mathrm{d}z. \tag{4.8}$$

Proof. Due to $F_{K,\sigma} = -F_{L,\sigma}$ for $\sigma = K|L \in \mathcal{E}_{\mathrm{int}}$, and since $F_{K,\sigma} = 0$ for $\sigma \in \mathcal{E}(\partial\Omega)$ according to (3.3), we obtain by re-indexing the sum over all $\sigma \in \mathcal{E}_{\mathrm{int}}$:

$$\begin{aligned} \sum_{K\in\mathcal{K}} \sum_{\substack{\sigma\in\mathcal{E}(K)\\ \sigma\in\mathcal{E}_{\mathrm{int}}}} F_{K,\sigma} c_K = \sum_{\substack{\sigma\in\mathcal{E}_{\mathrm{int}}\\ \sigma=K|L}} F_{K,\sigma} c_K + F_{L,\sigma} c_L &= \sum_{\substack{\sigma\in\mathcal{E}_{\mathrm{int}}\\ \sigma=K|L}} F_{K,\sigma}(c_K - c_L) \\ &= \sum_{\sigma\in\mathcal{E}_{\mathrm{int}}} \tau_\sigma \left(D_\sigma c_h\right)^2 = \|c_h\|_{1,\mathcal{K}}^2. \end{aligned}$$

Furthermore, since $V_{K,\sigma} = -V_{L,\sigma}$, we have

$$\begin{aligned} \sum_{K\in\mathcal{K}} \sum_{\sigma\in\mathcal{E}(K)} V_{K,\sigma} c_K &= \sum_{\substack{\sigma\in\mathcal{E}_{\mathrm{int}}\\ \sigma=K|L}} V_{K,\sigma}(c_K - c_L) + \sum_{\substack{\sigma\in\mathcal{E}(\partial\Omega)\\ \sigma\in\mathcal{E}(K)}} V_{K,\sigma} c_K \\ &= \sum_{\substack{\sigma\in\mathcal{E}_{\mathrm{int}}\\ \sigma=K|L}} u_{K,\sigma} c_{\sigma,+}(c_K - c_L) + \sum_{\substack{\sigma\in\mathcal{E}(\partial\Omega)\\ \sigma\in\mathcal{E}(K)}} u_{K,\sigma}\, c_K^2, \end{aligned} \tag{4.9}$$

where the latter sum vanishes due to $c_K = 0$ for $K \in \mathcal{K}(\Gamma)$ and $u_{K,\sigma} = 0$ for $\sigma \subset \Gamma_{\mathrm{rot}}$ because $\boldsymbol{u}$ is axisymmetric. Due to the definition of $c_{\sigma,\pm}$ in (3.5), we have

$$\begin{aligned} u_{K,\sigma} c_{\sigma,+}(c_K - c_L) &= \begin{cases} u_{K,\sigma} c_{\sigma,+}(c_K - c_L) & \text{if } u_{K,\sigma} \geq 0, \\ -u_{K,\sigma} c_{\sigma,+}(c_L - c_K) & \text{if } u_{K,\sigma} < 0 \end{cases} \\ &= \begin{cases} u_{K,\sigma} c_{\sigma,+}(c_{\sigma,+} - c_{\sigma,-}) & \text{if } u_{K,\sigma} \geq 0, \\ -u_{K,\sigma} c_{\sigma,+}(c_{\sigma,+} - c_{\sigma,-}) & \text{if } u_{K,\sigma} < 0 \end{cases} \\ &= |u_{K,\sigma}| c_{\sigma,+}(c_{\sigma+} - c_{\sigma,-}). \end{aligned}$$

Thus, in any case, we have that

$$\sum_{\substack{\sigma\in\mathcal{E}_{\mathrm{int}}\\ \sigma=K|L}} u_{K,\sigma} c_{\sigma,+}(c_K - c_L) = \sum_{\substack{\sigma\in\mathcal{E}_{\mathrm{int}}\\ \sigma=K|L}} |u_{K,\sigma}| c_{\sigma,+}(c_{\sigma,+} - c_{\sigma,-}).$$

Consequently, we obtain:

$$\begin{aligned}\sum_{\substack{\sigma\in\mathcal{E}_{\mathrm{int}}\\ \sigma=K|L}} V_{K,\sigma}(c_K-c_L) &= \sum_{\substack{\sigma\in\mathcal{E}_{\mathrm{int}}\\ \sigma=K|L}} |u_{K,\sigma}| c_{\sigma,+}\,(c_{\sigma,+}-c_{\sigma,-})\\ &= \frac{1}{2}\sum_{\substack{\sigma\in\mathcal{E}_{\mathrm{int}}\\ \sigma=K|L}} |u_{K,\sigma}|\Big[\underbrace{(c_{\sigma,+}-c_{\sigma,-})^2}_{\geq 0}+(c_{\sigma,+}^2-c_{\sigma,-}^2)\Big]\\ &\geq \frac{1}{2}\sum_{\substack{\sigma\in\mathcal{E}_{\mathrm{int}}\\ \sigma=K|L}} |u_{K,\sigma}|\,(c_{\sigma,+}^2-c_{\sigma,-}^2).\end{aligned}$$

Since $|u_{K,\sigma}|\,(c_{\sigma,+}^2-c_{\sigma,-}^2)=u_{K,\sigma}c_K^2+u_{L,\sigma}c_L^2$, we continue with

$$\begin{aligned}\sum_{K\in\mathcal{K}}\sum_{\sigma\in\mathcal{E}(K)} V_{K,\sigma}c_K &\geq \frac{1}{2}\sum_{\substack{\sigma\in\mathcal{E}_{\mathrm{int}}\\ \sigma=K|L}} u_{K,\sigma}c_K^2+u_{L,\sigma}c_L^2\\ &= \frac{1}{2}\sum_{K\in\mathcal{K}}\left(\int_{\partial K} r\,\boldsymbol{u}\cdot\boldsymbol{n}_K\,\mathrm{d}S\right)c_K^2\\ &= \frac{1}{2}\int_\Omega \mathrm{div}_{(r,z)}(r\boldsymbol{u})\,c_h^2\,\mathrm{d}r\,\mathrm{d}z.\end{aligned}$$

This concludes the proof. □

Remark 4.4 (Stability)**.** Based on Lemma 4.3, one can show a stability estimate in a similar manner as in [EGH00, Lemma 9.2] and [FLL11b, Lemma 3.9].

We now extend the error estimates presented in [GHV00] to our axisymmetric setting.

Theorem 4.5 (H_1^2 Error Estimate)**.** For $g\in H_1^{3/2}(\Gamma)$ and $c\in H_1^2(\Omega)$, the discrete solution $c_h=(c_K)_{K\in\mathcal{K}}$ of (3.1)–(3.2) and the error $e_h=(e_K)_{K\in\mathcal{K}}\in W_{h,0}(\mathcal{K})$ defined by $e_K:=c(x_K)-c_K$ for $K\in\mathcal{K}$ satisfy

$$\|e_h\|_{1,\mathcal{K}}\leq C\,\mathrm{size}(\mathcal{K}) \quad \text{and} \tag{4.10}$$

$$\|e_h\|_{L_1^2(\Omega)}\leq C\,\mathrm{size}(\mathcal{K}). \tag{4.11}$$

Here, $C\in\mathbb{R}$ depends only on c, $\boldsymbol{u}$, Ω and the shape constant

$$\zeta:=\min_{K\in\mathcal{K}}\min_{\sigma\in\mathcal{E}(K)}\frac{d_{K,\sigma}}{\mathrm{diam}(K)}. \tag{4.12}$$

Proof. The L_1^2-estimate (4.11) is a direct consequence of the discrete Poincaré inequality (4.3) and Lemma 4.1. The remaining proof of (4.10) consists of two steps. Step 1 concerns the consistency of the flux approximation and Step 2 establishes the error estimates.

Step 1: Consistency. For a given control volume $K\in\mathcal{K}$ and edge $\sigma\in\mathcal{E}(K)\cap\mathcal{E}_{\mathrm{int}}$, we define the exact diffusion flux $\overline{F}_{K,\sigma}$ and the exact convection flux $\overline{V}_{K,\sigma}$ by

$$\begin{aligned}\overline{F}_{K,\sigma}&:=-\int_\sigma r(x)\,\nabla c(x)\cdot\boldsymbol{n}_{K,\sigma}\,\mathrm{d}S(x),\\ \overline{V}_{K,\sigma}&:=\int_\sigma r(x)\,c(x)\boldsymbol{u}(x)\cdot\boldsymbol{n}_{K,\sigma}\,\mathrm{d}S(x).\end{aligned} \tag{4.13}$$

Let us also define the discrete fluxes

$$F^*_{K,\sigma} := -\tau_\sigma\left(c(x_L) - c(x_K)\right) = -\frac{c(x_L)-c(x_K)}{d_\sigma}\int_\sigma r(x)\,\mathrm{d}S,$$

$$\text{where } \tau_\sigma := \begin{cases} |\sigma| r(\mathrm{mid}(\sigma))/d_\sigma & \text{if } \sigma = K|L \\ 0 & \text{else} \end{cases}, \tag{4.14}$$

$$V^*_{K,\sigma} := u_{K,\sigma}\, c(x_{\sigma,+}),$$

$$\text{where } x_{\sigma,+} := \begin{cases} x_K, & \text{if } u_{K,\sigma} \geq 0, \\ x_L, & \text{if } u_{K,\sigma} < 0. \end{cases} \tag{4.15}$$

Their differences define the consistency errors

$$R_{K,\sigma} := \frac{1}{|\sigma| r(\mathrm{mid}(\sigma))}\left(\overline{F}_{K,\sigma} - F^*_{K,\sigma}\right) \text{ and } r_{K,\sigma} := \frac{1}{|\sigma| r(\mathrm{mid}(\sigma))}\left(\overline{V}_{K,\sigma} - V^*_{K,\sigma}\right). \tag{4.16}$$

We also denote the diamond co-volume at $\sigma = K|L \in \mathcal{E}_{\mathrm{int}}$ by $\mathcal{V}_\sigma := \mathcal{V}_{K,\sigma} \cup \mathcal{V}_{L,\sigma}$ where $\mathcal{V}_{K,\sigma} := \{tx_K + (1-t)x \,|\, x \in \sigma, t \in [0,1]\}$ The goal is to derive constants C_1 and C_2 depending on $\boldsymbol{u}, \zeta$, and $p > 3$ such that, for all neighbouring volumes $K, L \in \mathcal{K}$, and $\sigma = K|L \in \mathcal{E}_{\mathrm{int}}$,

$$|R_{K,\sigma}| \leq C_1 \max\{\mathrm{diam}(K), \mathrm{diam}(L)\}\left(|\sigma| r(\mathrm{mid}(\sigma)) d_\sigma\right)^{-1/2} \|c\|_{H^2_1(\mathcal{V}_\sigma)}, \tag{4.17}$$

$$|r_{K,\sigma}| \leq C_2 \max\{\mathrm{diam}(K), \mathrm{diam}(L)\}\left(|\sigma| r(\mathrm{mid}(\sigma)) d_\sigma\right)^{-1/p} \|c\|_{W^{1,p}_1(\mathcal{V}_\sigma)}. \tag{4.18}$$

Since $c \in H^2_1(\mathcal{V}_\sigma)$ and $C^\infty(\overline{\mathcal{V}_\sigma})$ is dense in $H^2_1(\mathcal{V}_\sigma)$, see e.g. [Kuf85, Theorem 11.2], it suffices to show these estimates for $c \in C^\infty(\overline{\mathcal{V}_\sigma})$. Now two Taylor expansions of c around $x \in \sigma$ read

$$c(x_L) = c(x) + \nabla c(x)\cdot(x_L - x) + \int_0^1 D^2 c(tx + (1-t)x_L)(x_L - x)^2\, t\,\mathrm{d}t,$$
$$c(x_K) = c(x) + \nabla c(x)\cdot(x_K - x) + \int_0^1 D^2 c(tx + (1-t)x_K)(x_K - x)^2\, t\,\mathrm{d}t.$$

Multiplication with $r(x)/d_\sigma$, subtracting the second one from the first, integration over σ, and $x_L - x_K = d_\sigma \boldsymbol{n}_{K,\sigma}$ yields We multiply both equations with $r(x)$ and subtract the second one from the first.

$$\overbrace{\frac{c(x_L)-c(x_K)}{d_\sigma}\int_\sigma r(x)\,\mathrm{d}S}^{-F^*_{K,\sigma}} = \overbrace{\int_\sigma r(x)\nabla c(x)\cdot\boldsymbol{n}_{K,\sigma}\,\mathrm{d}S}^{-\overline{F}_{K,\sigma}}$$
$$+ \frac{1}{d_\sigma}\int_\sigma r(x)\int_0^1 D^2 c(tx + (1-t)x_L)(x_L - x)^2\, t\,\mathrm{d}t\,\mathrm{d}S,$$
$$- \frac{1}{d_\sigma}\int_\sigma r(x)\int_0^1 D^2 c(tx + (1-t)x_K)(x_K - x)^2\, t\,\mathrm{d}t\,\mathrm{d}S.$$

We set $x_t := tx + (1-t)x_K$ so that $|R_{K,\sigma}| \leq B_{K,\sigma} + B_{L,\sigma}$ where

$$B_{K,\sigma} := \frac{1}{d_\sigma |\sigma| r(\mathrm{mid}(\sigma))}\left|\int_\sigma r(x)\int_0^1 D^2 c(x_t)(x_K - x)^2\, t\,\mathrm{d}t\,\mathrm{d}S\right|.$$

Since $|x_K - x| \leq \mathrm{diam}(K)$, we have

$$B_{K,\sigma} \leq \frac{\mathrm{diam}(K)^2}{d_\sigma |\sigma| r(\mathrm{mid}(\sigma))}\int_\sigma r(x)\int_0^1 \left|D^2 c(x_t)\right|\, t\,\mathrm{d}t\,\mathrm{d}S, \tag{4.19}$$

where $|D^2 c(z)|$, $z \in \mathcal{V}_{K,\sigma}$ denotes the induced operator norm of $D^2 c(z)$.

To bound $B_{K,\sigma}$ by $\|c\|_{H_1^2(\mathcal{V}_{K,\sigma})}$, we need to relate $r(x)$ to $r(x_t)$. Since $r(x_t) = r(x_K)+t(r(x)-r(x_K))$, we have $tr(x) = r(x_t) + (t-1)r(x_K)$ and due to $(t-1)r(x_K) \leq 0$ we obtain

$$tr(x) \leq r(x_t). \tag{4.20}$$

Now as $t \leq 1$, by using (4.20) and the Cauchy–Schwarz inequality, we proceed from (4.19):

$$\begin{aligned} B_{K,\sigma} &\leq \frac{\operatorname{diam}(K)^2}{d_\sigma |\sigma| r(\operatorname{mid}(\sigma))} \int_\sigma \int_0^1 r(x)^{1/2} r(x_t)^{1/2} |D^2 c(x_t)| t^{1/2} \,\mathrm{d}t \,\mathrm{d}S \\ &\leq \frac{\operatorname{diam}(K)^2}{d_\sigma |\sigma| r(\operatorname{mid}(\sigma))} \underbrace{\left(\int_\sigma r(x) \int_0^1 \mathrm{d}t \,\mathrm{d}S \right)^{1/2}}_{=(|\sigma| r(\operatorname{mid}(\sigma)))^{1/2}} \left(\int_\sigma \int_0^1 r(x_t) |D^2 c(x_t)|^2 \, t \,\mathrm{d}t \,\mathrm{d}S \right)^{1/2} \\ &= \frac{\operatorname{diam}(K)^2}{d_\sigma \left(|\sigma| r(\operatorname{mid}(\sigma))\right)^{1/2}} \left(\int_\sigma \int_0^1 r(x_t) |D^2 c(x_t)|^2 \, t \,\mathrm{d}t \,\mathrm{d}S \right)^{1/2}. \end{aligned} \tag{4.21}$$

We now parametrize σ such that $x \in \sigma$ is expressed as $x = x_b + s\boldsymbol{\tau}_\sigma$, $s \in [0, |\sigma|]$ for a tangent vector $\boldsymbol{\tau}_\sigma \perp \boldsymbol{n}_{K,\sigma}$ and an end point $x_b \in \sigma$. Any point $z \in \mathcal{V}_{K,\sigma}$ can thus be written as $z = \varphi(s,t) := tx_b + ts\boldsymbol{\tau}_\sigma + (1-t)x_K$ for the mapping $\varphi : [0, |\sigma|] \times [0,1] \to \mathcal{V}_{K,\sigma}$. Substituting $z = \varphi(s,t)$ in (4.21) yields

$$B_{K,\sigma} \leq \frac{\operatorname{diam}(K)^2}{d_\sigma \left(|\sigma| r(\operatorname{mid}(\sigma))\right)^{1/2}} d_{K,\sigma}^{-1/2} \left(\int_{\mathcal{V}_{K,\sigma}} r(z) \left| D^2 c(z) \right|^2 \mathrm{d}z \right)^{1/2}. \tag{4.22}$$

Now due to $d_{K,\sigma}$, $d_{L,\sigma} \geq \zeta \operatorname{diam}(K)$, (4.22) implies

$$B_{K,\sigma} \leq \frac{\operatorname{diam}(K)}{\zeta \left(d_\sigma |\sigma| r(\operatorname{mid}(\sigma))\right)^{1/2}} \|c\|_{H_1^2(\mathcal{V}_{K,\sigma})}.$$

A similar estimate for $B_{L,\sigma}$ and the inequality $(a+b)^2 \leq 2\left(a^2+b^2\right)$ yields (4.17) with $C_1 = \sqrt{2}/\zeta$ for $c \in C^2(\Omega)$. A density argument extends the result to $c \in H_1^2(\Omega)$.

For the proof of (4.18), we assume w.l.o.g. $u_{K,\sigma} \geq 0$ such that $x_{\sigma,+} = x_K$ (the proof continues analogously if $u_{K,\sigma} < 0$) and expand $c \in C^1(\overline{\mathcal{V}_{K,\sigma}})$ for $x \in \sigma$ by

$$c(x) = c(x_K) + \int_0^1 \nabla c(tx + (1-t)x_K)(x - x_K) \,\mathrm{d}t.$$

Let now $p > 3$ and $q \in \mathbb{R}$ its conjugate such that $1/p + 1/q = 1$. Plugging the expansion into $r_{K,\sigma}$, (4.20) and a Hölder inequality results in

$$\begin{aligned} |r_{K,\sigma}| &\leq \left(|\sigma| r(\operatorname{mid}(\sigma))\right)^{-1} \int_\sigma \int_0^1 r(x) \left| \boldsymbol{u}(x) \cdot \boldsymbol{n}_{K,\sigma} \right| |\nabla c(x_t)| \, d_{K,\sigma} \,\mathrm{d}t \,\mathrm{d}S(x) \\ &\leq \left(|\sigma| r(\operatorname{mid}(\sigma))\right)^{-1} \|\boldsymbol{u}\|_{L^\infty(\Omega)} d_{K,\sigma} \int_\sigma \int_0^1 r(x)^{1/q} r(x_t)^{1/p} t^{-2/p} t^{1/p} |\nabla c(x_t)| \,\mathrm{d}t \,\mathrm{d}S(x) \\ &\leq \left(|\sigma| r(\operatorname{mid}(\sigma))\right)^{-1} \|\boldsymbol{u}\|_{L^\infty(\Omega)} d_{K,\sigma} \left(\int_\sigma \int_0^1 r(x) \, t^{-2q/p} \,\mathrm{d}t \,\mathrm{d}S(x) \right)^{1/q} \\ &\quad \times \left(\int_\sigma \int_0^1 r(x_t) \left| \nabla c(x_t) \right|^p t \,\mathrm{d}t \,\mathrm{d}S(x) \right)^{1/p}. \end{aligned}$$

The latter term yields the semi-norm $|c|_{W_1^{1,p}(\mathcal{V}_{K,\sigma})}$, while the former integral exists due to $q/p < \frac{1}{2}$. More precisely, we have

$$\int_\sigma r(x) \int_0^1 t^{-2q/p} \,\mathrm{d}t \,\mathrm{d}S(x) = \frac{1}{1-2q/p} \int_\sigma r(x) \,\mathrm{d}S(x) = \frac{|\sigma| r(\mathrm{mid}(\sigma))}{1-2q/p}.$$

In total, setting $C_2 := \|u\|_{L^\infty(\Omega)} \, (1-2q/p)^{-1/q}$ and observing $1-1/p > 2/3$ so that $d_{K,\sigma}^{1-1/p} \leq d_\sigma^{1-1/p}$, we arrive at

$$\begin{aligned} |r_{K,\sigma}| &\leq C_2 \left(|\sigma| r(\mathrm{mid}(\sigma))\right)^{-1+1/q} d_{K,\sigma}^{1-1/p} \|c\|_{W_1^{1,p}(\mathcal{V}_\sigma)} \\ &\leq C_2 \,\mathrm{diam}(K) \left(|\sigma| r(\mathrm{mid}(\sigma) d_\sigma)\right)^{-1/p} \|c\|_{W_1^{1,p}(\mathcal{V}_\sigma)}, \end{aligned}$$

which concludes the proof of (4.18).

Step 2: Error estimate. Since $c \in H_1^2(\Omega)$ is the variational solution satisfying (2.3), testing with the characteristic functions of the control volumes leads to

$$\sum_{\sigma \in \mathcal{E}(K)} \left(\overline{F}_{K,\sigma} + \overline{V}_{K,\sigma}\right) = \int_K r \, s \,\mathrm{d}r \,\mathrm{d}z \quad \text{for all } K \in \mathcal{K} \setminus \mathcal{K}(\Gamma). \tag{4.23}$$

As c is also continuous, $F_{K,\sigma}^*$, $V_{K,\sigma}^*$ from (4.14), (4.15) are well-defined. Subtracting (3.1) from (4.23), summing over all $K \in \mathcal{K}$, and multiplying by e_K yields

$$\begin{aligned} \sum_{K\in\mathcal{K}} \sum_{\sigma\in\mathcal{E}(K)} \left(F_{K,\sigma}^* - F_{K,\sigma}\right) e_K + \left(V_{K,\sigma}^* - V_{K,\sigma}\right) e_K \\ = - \sum_{K\in\mathcal{K}} \sum_{\sigma\in\mathcal{E}(K)} |\sigma| \, r(\mathrm{mid}(\sigma)) \left(R_{K,\sigma} + r_{K,\sigma}\right) e_K. \end{aligned} \tag{4.24}$$

Similar to the downwind value $c_{\sigma,-}$ of c_h, we introduce the downwind node

$$x_{\sigma,-} := \begin{cases} x_L, & \text{if } u_{K,\sigma} \geq 0 \\ x_K, & \text{if } u_{K,\sigma} < 0 \end{cases}$$

and analogously the upwind and downwind errors across σ via

$$e_{\sigma,+} := c(x_{\sigma,+}) - c_{\sigma,+} \quad \text{and} \quad e_{\sigma,-} := c(x_{\sigma,-}) - c_{\sigma,-}.$$

We can now apply Lemma 4.3 to the left-hand side of (4.24) with the modified error-fluxes $F_{K,\sigma}(e_h) := F_{K,\sigma}^* - F_{K,\sigma}$ and $V_{K,\sigma}(e_h) := V_{K,\sigma}^* - V_{K,\sigma}$, which yields

$$\|e_h\|_{1,\mathcal{K}}^2 + \frac{1}{2} \int_\Omega \mathrm{div}_{(r,z)}(r\boldsymbol{u}) \, e_h^2 \,\mathrm{d}r \,\mathrm{d}z \leq - \sum_{K\in\mathcal{K}} \sum_{\sigma\in\mathcal{E}(K)} |\sigma| \, r(\mathrm{mid}(\sigma)) \left(R_{K,\sigma} + r_{K,\sigma}\right) e_K. \tag{4.25}$$

We now turn to the right-hand side. Due to the conservativity of the scheme, we have $R_{K,\sigma} = -R_{L,\sigma}$, and $r_{L,\sigma} = -r_{L,\sigma}$ and again reordering over the edges, we obtain using Young's inequality and $(|R_{K,\sigma}| +$

$$|r_{K,\sigma}|)^2 \le 2(|R_{K,\sigma}|^2 + |r_{K,\sigma}|^2)$$

$$\sum_{K\in\mathcal{K}} \sum_{\sigma\in\mathcal{E}(K)} |\sigma|\, r(\mathrm{mid}(\sigma))\,(R_{K,\sigma} + r_{K,\sigma})\, e_K = \sum_{\substack{\sigma\in\mathcal{E}_{\mathrm{int}}\\ \sigma=K|L}} |\sigma|\, r(\mathrm{mid}(\sigma))\,(R_{K,\sigma} + r_{K,\sigma})\,(e_K - e_L)$$

$$\le \sum_{\substack{\sigma\in\mathcal{E}_{\mathrm{int}}\\ \sigma=K|L}} |\sigma|\, r(\mathrm{mid}(\sigma))\ (|R_{K,\sigma}| + |r_{K,\sigma}|)\, D_\sigma e_h$$

$$\le \frac{1}{2} \sum_{\substack{\sigma\in\mathcal{E}_{\mathrm{int}}\\ \sigma=K|L}} \frac{|\sigma| r(\mathrm{mid}(\sigma))}{d_\sigma}\,(D_\sigma e_h)^2 + \sum_{\substack{\sigma\in\mathcal{E}_{\mathrm{int}}\\ \sigma=K|L}} |\sigma| r(\mathrm{mid}(\sigma)) d_\sigma |R_{K,\sigma}|^2$$

$$+ \sum_{\substack{\sigma\in\mathcal{E}_{\mathrm{int}}\\ \sigma=K|L}} |\sigma| r(\mathrm{mid}(\sigma)) d_\sigma |r_{K,\sigma}|^2.$$

We now apply (4.17) yielding

$$\sum_{\substack{\sigma\in\mathcal{E}_{\mathrm{int}}\\ \sigma=K|L}} |\sigma| r(\mathrm{mid}(\sigma)) d_\sigma |R_{K,\sigma}|^2 \le C_1^2\, \mathrm{size}(\mathcal{K})^2 \sum_{\substack{\sigma\in\mathcal{E}_{\mathrm{int}}\\ \sigma=K|L}} \|c\|^2_{H_1^2(\mathcal{V}_\sigma)} = C_1^2\, \mathrm{size}(\mathcal{K})^2\, \|c\|^2_{H_1^2(\Omega)}.$$

Using (4.18) and Hölder's inequality with exponents $p/(p-2)$ and $p/2$ applied to the remaining sum, we obtain

$$\sum_{\substack{\sigma\in\mathcal{E}_{\mathrm{int}}\\ \sigma=K|L}} |\sigma| r(\mathrm{mid}(\sigma)) d_\sigma |r_{K,\sigma}|^2 \le C_2^2\, \mathrm{size}(\mathcal{K})^2 \sum_{\substack{\sigma\in\mathcal{E}_{\mathrm{int}}\\ \sigma=K|L}} (|\sigma| r(\mathrm{mid}(\sigma)) d_\sigma)^{1-2/p}\, \|c\|^2_{W_1^{1,p}(\mathcal{V}_\sigma)}$$

$$\le C_2^2\, \mathrm{size}(\mathcal{K})^2 \Bigg(\sum_{\substack{\sigma\in\mathcal{E}_{\mathrm{int}}\\ \sigma=K|L}} |\sigma|\, r(\mathrm{mid}(\sigma))\, d_\sigma \Bigg)^{\frac{p-2}{p}} \Bigg(\sum_{\substack{\sigma\in\mathcal{E}_{\mathrm{int}}\\ \sigma=K|L}} \|c\|^p_{W_1^{1,p}(\mathcal{V}_\sigma)} \Bigg)^{2/p}$$

$$\le C_2^2\, \mathrm{size}(\mathcal{K})^2\ (\mathrm{diam}(\Omega)\, |\Omega|)^{\frac{p-2}{p}}\, \|c\|^2_{W_1^{1,p}(\Omega)},$$

where we used $\sum_{\sigma\in\mathcal{E}_{\mathrm{int}}} |\sigma|\, d_\sigma = 2\sum_{\sigma\in\mathcal{E}_{\mathrm{int}}} |\mathcal{V}_\sigma| = 2|\Omega|$. Since $\mathrm{div}_{(r,z)}(r\,\boldsymbol{u}) = \mathrm{div}_x\, \widehat{\boldsymbol{u}} = 0$, combining the previous results with (4.25), we obtain

$$\|e_h\|_{1,\mathcal{K}} \le \widetilde{C}\, \mathrm{size}(\mathcal{K})$$

where $\widetilde{C}^2 := \max\Big\{ C_1^2\, \|c\|^2_{H_1^2(\Omega)}, C_2^2\ (\mathrm{diam}(\Omega)\, |\Omega|)^{\frac{p-2}{p}}\, \|c\|^2_{W_1^{1,p}(\Omega)} \Big\}$. This concludes the proof. □

5. Extension to Mixed Boundary Conditions

This section studies the axisymmetric formulation of the transport equations under mixed boundary conditions. We assume a split of the domain boundary into $\Gamma = \Gamma_{\mathrm{D}} \cup \Gamma_{\mathrm{R}}$ where Γ_{D} denotes the (closed) Dirichlet boundary part and $\Gamma_{\mathrm{R}} := \Gamma \setminus \Gamma_{\mathrm{D}}$ denotes the Robin boundary part. On Γ_{D} and Γ_{R}, we expect Dirichlet and Robin boundary conditions, respectively, i.e.,

$$\begin{aligned} c(x) &= g_D(x), \quad x \in \Gamma_{\mathrm{D}}, \\ -\boldsymbol{j}_{\mathrm{cyl}}(c)\cdot\boldsymbol{n} + \lambda(x)c(x) &= g_R(x), \quad x \in \Gamma_{\mathrm{R}} \end{aligned} \tag{5.1}$$

for given data $g_D \in H^{1/2}(\Gamma_{\mathrm{D}})$, $g_R \in H^{1/2}(\Gamma_{\mathrm{R}})$, and a weight function $\lambda \in L^\infty(\Omega)$ with

$$\frac{1}{2}\,\boldsymbol{u}\cdot\boldsymbol{n} + \lambda \ge 0 \text{ on } \Gamma_{\mathrm{R}}. \tag{5.2}$$

The weak formulation retrieved from modifying (2.3) seeks $c \in g_D + H^1_{1,D}(\Omega) := \{\phi \in H^1_1(\Omega) : \phi|_{\Gamma_\mathrm{D}} = 0\}$ such that

$$\int_\Omega r\,[D\nabla c\cdot\nabla\phi + \boldsymbol{u}\cdot\nabla c\,\phi]\,\mathrm{d}r\,\mathrm{d}z + \int_{\Gamma_\mathrm{R}} r\,\lambda\,c\,\phi\;\mathrm{d}S(r,z) = \int_{\Gamma_\mathrm{R}} r\,g_R\phi(x)\,\mathrm{d}S(r,z) + \int_\Omega rs\,\phi\,\mathrm{d}r\,\mathrm{d}z \quad \text{for all } \phi \in H^1_{1,D}(\Omega). \tag{5.3}$$

Under condition (5.2), the Lax-Milgram theorem guarantees a unique solution.

For some qualitative results beyond unique existence, we assume additionally

$$\lambda - \frac{1}{2}\boldsymbol{u}\cdot\boldsymbol{n} \geq 0 \quad \text{on } \Gamma_R, \tag{5.4}$$

$$\lambda - \boldsymbol{u}\cdot\boldsymbol{n} \geq 0 \quad \text{on } \Gamma_R. \tag{5.5}$$

Assumption (5.4) is needed to establish the error estimate in Theorem 5.4, while assumption (5.5) is needed to establish a discrete min/max principle, see Remark 5.2.

Remark 5.1 (Examples for mixed boundary conditions)**.** The convection-diffusion system can be used to model e.g. heterogeneous catalysis. Here, the Dirichlet boundary may represent an inlet with a prescribed inlet mass density. Inert and outflow boundary conditions are realized by $g_R(x) = 0$ and $\lambda(x) = \boldsymbol{u}\cdot\boldsymbol{n}$. Reaction boundary conditions at the electrode or catalyst are of the form $\lambda(x) = 0$ and $g_R(x) = R(x)$ for some catalytic response function R.

If it can be assumed that the velocity $\boldsymbol{u}$ is directed outward almost everywhere at the reactor outlet, i.e. $\boldsymbol{u}\cdot\boldsymbol{n} \geq 0$, and that $\boldsymbol{u}$ satisfies no-slip boundary conditions at the catalyst so that $\boldsymbol{u}\cdot\boldsymbol{n} = 0$, then condition (5.2) also implies (5.4) and (5.5).

5.1. **Discrete system.** Keeping the notation of the fluxes from (3.1), one seeks $c_h \in P_0(\mathcal{K})$ such that, for all $K \in \mathcal{K} \setminus \mathcal{K}(\Gamma_\mathrm{D})$,

$$\sum_{\sigma\in\mathcal{E}(K)\cap\mathcal{E}(\Omega)} (F_{K,\sigma} + V_{K,\sigma}) + \sum_{\sigma\in\mathcal{E}(K)\cap\mathcal{E}(\Gamma_\mathrm{R})} N_{K,\sigma} = s_K + \sum_{\sigma\in\mathcal{E}(K)\cap\mathcal{E}(\Gamma_\mathrm{R})} g_\sigma \tag{5.6}$$

where the Robin boundary condition gives rise to the additional terms

$$g_\sigma := \int_\sigma r\,g_R\,\mathrm{d}S(r,z) \text{ and } N_{K,\sigma} := c_K \int_\sigma r\,\lambda\,\mathrm{d}S(r,z) \text{ for } K \in \mathcal{K}, \sigma \in \mathcal{E}(K)\cap\mathcal{E}(\Gamma_\mathrm{R}).$$

For boundary volumes $K \in \mathcal{K}(\Gamma_\mathrm{D})$, we keep the Dirichlet boundary condition from (3.2).

Remark 5.2 (Min/max principles)**.** Note, that the local and global min/max principles still hold, under the conditions (5.5) and (3.8), if additionally $g_R \leq 0$ (or $g_R \geq 0$). The modifications to the proof of Theorem 3.3 are straightforward.

5.2. **Error analysis.** In order to show similar error bounds as in the previous section, we need to extend some discrete inequalities from [GHV00] to weighted Sobolev norms. Careful argumentation is needed in the vicinity of the axis of revolution. Since the Dirichlet boundary Γ_D is only a subset of Γ, the discrete space $W_h(\mathcal{K})$ from (4.1) is modified to

$$W_h(\mathcal{K}) := \{c_h \in P_0(\mathcal{K}) : c_h|_K = 0 \quad \text{for } K \in \mathcal{K}(\Gamma_\mathrm{D})\}\,.$$

It approximates $H^1_{1,D}(\Omega)$ and $\|\bullet\|_{1,\mathcal{K}}$ is still a norm on this space.

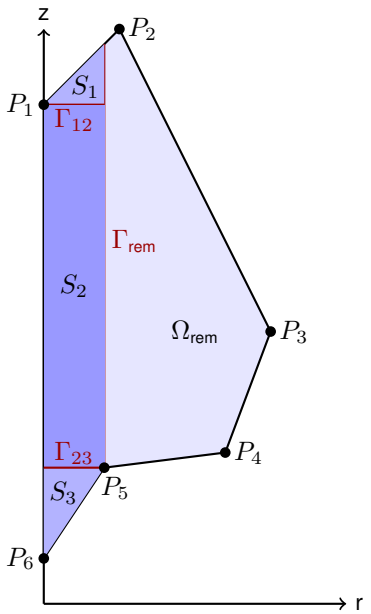

FIGURE 5.1. Splitting of the domain into $\Omega_{\text{rot}} = S_1 \cup S_2 \cup S_3$ and Ω_{rem} as described in the proof of Lemma 5.3.

Lemma 5.3 (Discrete Poincaré Inequality with Boundary Contribution)**.** There exists a $C \in \mathbb{R}$ only depending on Ω such that

$$\|c_h\|_{L^2_1(\Omega)} \leq C \left(|c_h|^2_{1,\mathcal{K}} + \|c_h\|^2_{L^2_1(\Gamma_{\mathrm{D}})} \right) \quad \text{for any } c_h \in P_0(\mathcal{K}). \tag{5.7}$$

Proof. A proof can be devised by slightly adjusting the original ideas presented in [GHV00] to accommodate the weight r close to the axis of revolution Γ_{rot}. Therefore, only a sketch of the proof is provided.

The boundary $\partial\Omega$ is composed of line segments connecting the points $P = (P_1, \ldots, P_N), P_j = (r_j, z_j)$ for some $N \in \mathbb{N}$. Denote by

$$r_{\min} := \min_{j \in \{1,\ldots,N\}, r_j > 0} r_j = r_{j_{\min}} \quad \text{for} \quad P_{j_{\min}} = (r_{\min}, z_{j_{\min}})$$

the minimal r-coordinate of all the points in P. We then denote by Ω_{rot} the strip $\Omega_{\mathrm{rot}} := ((0, r_{\min}/2) \times \mathbb{R}) \cap \Omega$ contained in Ω left of $\{r_{\min}/2\} \times \mathbb{R}$ and the remainder $\Omega_{\mathrm{rem}} := \Omega \setminus \Omega_{\mathrm{rot}}$ which has a guaranteed minimal distance to the axis of revolution to allow for classical estimates.

We further decompose the strip Ω_{rot} into the sets $\Omega_{\mathrm{rot}} = S_1 \cup S_2 \cup S_3$, where the segments separating S_j and S_{j+1}, $j \in \{1, 2\}$ are given by $\Gamma_{ij} := \partial S_i \cap \partial S_j$ and the shared segment between Ω_{rot} and Ω_{rem} is denoted by $\Gamma_{\mathrm{rem}} := \partial\Omega_{\mathrm{rot}} \cap \partial\Omega_{\mathrm{rem}}$, see Figure 5.1. Crucially, on each subdomain S_j, it holds that almost all $x \in S_j$ lie on a line segment along $\pm \boldsymbol{e}_r$ or $\pm \boldsymbol{e}_z$ intersecting Γ_{rem} or Γ_{ij} where applicable.

W.l.o.g. we require that Γ_{D} coincides with a subset of the line segments along the polygonal chain P. We can therefore distinguish between the two cases that either $\Gamma_{\mathrm{D}} \subset \partial\Omega_{\mathrm{rem}} \cap \partial\Omega$ or $\Gamma_{\mathrm{D}} \cap (\partial\Omega_{\mathrm{rem}} \cap \partial\Omega) = \emptyset$ and treat any combination of the cases separately.

We can now extend the trace and Poincaré inequalities from [GHV00, Lemmas 4.3, 4.4] to Ω_{rem} by virtue of a norm equivalence with constants $r_{\min}$ and $\operatorname{diam}(\Omega_{\mathrm{rem}})$ yielding

$$\|c_h\|^2_{L^2_1(\Omega_{\rm rem})} \leq C_1 \left(\|c_h\|^2_{1,\mathcal{K}} + \|\gamma c_h\|^2_{L^2_1(\Gamma_{\rm rem})} \right) \tag{5.8}$$

$$\|c_h\|^2_{L^2_1(\Gamma_{\rm rem})} \leq C_2 \left(\|c_h\|^2_{1,\mathcal{K}} + \|c_h\|^2_{L^2_1(\Omega_{\rm rem})} \right). \tag{5.9}$$

On the strip $\Omega_{\rm rot} = S_1 \cup S_2 \cup S_3$, we can derive trace and Poincaré inequalities in a similar fashion as in [GHV00, Lemma 4.4] and Lemma 4.1 by leveraging the fact that due to the rectangular shape of S_j, $j \in \{1,2,3\}$, we need only consider directions $\boldsymbol{d}, \boldsymbol{\eta} \in \{\pm \boldsymbol{e}_z, -\boldsymbol{e}_r\}$. This allows to show the following inequalities for $\widetilde{\Gamma} \in \{\Gamma_{12}, \Gamma_{23}, \Gamma_{\rm rem}\}$ where applicable with constants $C_3, C_4 \in \mathbb{R}$ depending only on Ω:

$$\|\gamma c_h\|^2_{L^2_1(\widetilde{\Gamma})} \leq C_3 \left(\|c_h\|^2_{1,\mathcal{K}} + \|c_h\|^2_{L^2_1(S_j)} \right), \tag{5.10}$$

$$\|c_h\|^2_{L^2_1(S_j)} \leq C_4 \left(\|c_h\|^2_{1,\mathcal{K}} + \|\gamma c_h\|^2_{L^2_1(\widetilde{\Gamma})} \right). \tag{5.11}$$

Finally, we can string together a series of the inequalities (5.8)–(5.11) to derive (5.7) by combining Poincaré inequalities on the subdomains $\Omega_{\rm rem}$ and $\Omega_{\rm rot}$ for each of the cases $\Gamma_D \subset \partial\Omega_{\rm rot} \cap \partial\Omega$ and $\Gamma_D \cap (\partial\Omega_{\rm rot} \cap \partial\Omega) = \emptyset$.

For instance, in the former case, if w.l.o.g. $\Gamma_{\rm D} \subset \partial S_1$, we can extract a Poincaré inequality for $\Omega_{\rm rem}$ by traversing through the subsets S_j of $\Omega_{\rm rot}$ according to

$$\begin{aligned}
\|c_h\|^2_{L^2_1(\Omega_{\rm rem})} &\overset{(5.8)}{\lesssim} \|c_h\|^2_{1,\mathcal{K}} + \|c_h\|^2_{L^2_1(\Gamma_{\rm rem})} \\
&\overset{(5.10)}{\lesssim} \|c_h\|^2_{1,\mathcal{K}} + \|c_h\|^2_{L^2_1(S_2)} \\
&\overset{(5.11)}{\lesssim} \|c_h\|^2_{1,\mathcal{K}} + \|c_h\|^2_{L^2_1(\Gamma_{12})} \\
&\overset{(5.10)}{\lesssim} \|c_h\|^2_{1,\mathcal{K}} + \|c_h\|^2_{L^2_1(S_1)} \\
&\overset{(5.11)}{\lesssim} \|c_h\|^2_{1,\mathcal{K}} + \|c_h\|^2_{L^2_1(\Gamma_D)}.
\end{aligned}$$

We can establish Poincaré inequalities of this kind for all subsets constituting Ω so that summing these yields (5.7). □

Theorem 5.4 (Error estimate for mixed boundary conditions)**.** Let $c_h \in P_0(\mathcal{K})$ be the solution of (5.6). Then there exists a constant $C \in \mathbb{R}$ depending only on c, g_R, $\boldsymbol{u}$, Ω, and ζ from (4.12) such that

$$\|e_h\|_{1,\mathcal{K}} \leq C \operatorname{size}(\mathcal{K}) \quad \text{and} \tag{5.12}$$

$$\|e_h\|_{L^2_1(\Omega)} \leq C \operatorname{size}(\mathcal{K}). \tag{5.13}$$

Proof. The strategy of the proof is similar to Theorem 4.5. This time an additional consistency error for the flux approximation $N_{K,\sigma}$ for the Robin boundary condition appears, namely

$$\begin{aligned}
\widetilde{R}_{K,\sigma} &:= \frac{1}{|\sigma|\, r_{\rm mid}(\sigma)} \left(\overline{N}_{K,\sigma} - N^\star_{K,\sigma} \right) \\
&:= \frac{1}{|\sigma|\, r_{\rm mid}(\sigma)} \int_\sigma \lambda(x) r (c(x) - c(x_K)) \,\mathrm{d}S(x) \\
&= \frac{1}{|\sigma|\, r_{\rm mid}(\sigma)} \int_\sigma \lambda(x) r \int_0^1 \nabla c(x_t)(x - x_K) \,\mathrm{d}t \,\mathrm{d}S(x),
\end{aligned}$$

where the last identity follows from a Taylor expansion argument. This can be estimated similarly to the convective fluxes in (4.18) and leads to

$$|\widetilde{R}_{K,\sigma}| \leq C_3 \operatorname{size}(\mathcal{K}) \left(|\sigma| r(\operatorname{mid}(\sigma)) d_\sigma\right)^{-1/p} \|\lambda\|_{L^\infty(\sigma)} \|c\|_{W^{1,p}(\mathcal{V}_\sigma)}.$$

for some C_3 depending only on $\boldsymbol{u}$, ζ, p.

A straightforward modification of (4.24) results in

$$\begin{aligned} &\sum_{K\in\mathcal{K}} \sum_{\sigma\in\mathcal{E}(K)} \left(F^*_{K,\sigma} - F_{K,\sigma}\right) e_K + \left(V^*_{K,\sigma} - V_{K,\sigma}\right) e_K + \sum_{\sigma\in\mathcal{E}(K)\cap\mathcal{E}(\Gamma_{\mathrm{R}})} \left(N^*_{K,\sigma} - N_{K,\sigma}\right) e_K \\ &= -\sum_{K\in\mathcal{K}} \sum_{\sigma\in\mathcal{E}(K)} |\sigma|\, r(\operatorname{mid}(\sigma)) \left(R_{K,\sigma} + r_{K,\sigma}\right) e_K - \sum_{\sigma\in\mathcal{E}(K)\cap\mathcal{E}(\Gamma_{\mathrm{R}})} |\sigma|\, r(\operatorname{mid}(\sigma)) \widetilde{R}_{K,\sigma} e_K. \end{aligned} \tag{5.14}$$

Another straightforward modification of Lemma 4.3 yields

$$\begin{aligned} &\sum_{K\in\mathcal{K}} \sum_{\sigma\in\mathcal{E}(K)} F_{K,\sigma} c_K + V_{K,\sigma} c_K + \sum_{\sigma\in\mathcal{E}(K)\cap\mathcal{E}(\Gamma_{\mathrm{R}})} N_{K,\sigma} c_K \\ &\qquad = \sum_{K\in\mathcal{K}} \sum_{\sigma\in\mathcal{E}(K)} F_{K,\sigma} c_K + V_{K,\sigma} c_K + \sum_{\sigma\in\mathcal{E}(K)\cap\mathcal{E}(\Gamma_{\mathrm{R}})} \left(V_{K,\sigma} + N_{K,\sigma} - V_{K,\sigma}\right) c_K \\ &\qquad \geq \|c_h\|^2_{1,\mathcal{K}} + \frac{1}{2}\left(\int_\Omega \operatorname{div}_{(r,z)}(r\boldsymbol{u})\, c_h^2 \,\mathrm{d}r\,\mathrm{d}z\right) + \int_{\Gamma_{\mathrm{R}}} \left(\lambda(x) - \frac{1}{2}\boldsymbol{u}\cdot\boldsymbol{n}\right) c_h^2 r \,\mathrm{d}S. \end{aligned}$$

A similar argument for the fluxes $F^\star_{K,\sigma} - F_{K,\sigma}$ for e_K instead of c_K and a combination with (5.14)

$$\begin{aligned} &\|e_h\|^2_{1,\mathcal{K}} + \frac{1}{2}\left(\int_\Omega \operatorname{div}_{(r,z)}(r\boldsymbol{u})\, e_h^2 \,\mathrm{d}r\,\mathrm{d}z\right) + \int_{\Gamma_{\mathrm{R}}} \left(\lambda(x) - \frac{1}{2}\boldsymbol{u}\cdot\boldsymbol{n}\right) e_h^2 r \,\mathrm{d}S \\ &\qquad \leq -\sum_{K\in\mathcal{K}} \sum_{\sigma\in\mathcal{E}(K)} |\sigma|\, r(\operatorname{mid}(\sigma)) \left(R_{K,\sigma} + r_{K,\sigma}\right) e_K - \sum_{\sigma\in\mathcal{E}(K)\cap\mathcal{E}(\Gamma_{\mathrm{R}})} |\sigma|\, r(\operatorname{mid}(\sigma)) \widetilde{R}_{K,\sigma} e_K. \end{aligned}$$

Since $\operatorname{div}_{(r,z)}(r\boldsymbol{u}) = 0$ and $\lambda(x) - \frac{1}{2}\boldsymbol{u}\cdot\boldsymbol{n} \geq 0$ according to (5.4), one can proceed as in Theorem 4.5 and this proves (5.12). It remains to show (5.13) which follows from the Poincaré inequality (5.7) derived in Lemma 5.3. □

6. Mass-conservative discretization of the axisymmetric Stokes problem

This section considers the axisymmetric formulation of the Stokes problem and its discretization by finite element methods. Moreover, a divergence-free postprocessing is suggested that allows to couple the discrete velocity field into the transport equation in a mass-conservative manner according to Theorem 3.3 and Remark 3.4.

6.1. FEM for the axisymmetric Stokes problem.

Recall the axisymmetric formulation of the Stokes problem from Section 2.4. For its finite element discretization, consider a pair of finite element spaces $\mathbf{V}_h \subset \mathbf{V}$ and $Q_h \subset Q$ with respect to a regular triangulation $\mathcal{T}$ that is not necessarily the same as for the finite volume discretization in Section 3. The set of polynomials of degree k on a triangle $T \in \mathcal{T}$ is denoted by $P_k(T)$, while the set of piecewise polynomials on $\mathcal{T}$ reads

$$P_k(\mathcal{T}) := \left\{q_h \in L^2(\Omega) : q_h|_T \in P_k(T) \text{ for all } T \in \mathcal{T}\right\}.$$

As usual their bold variant $\mathbf{P}_k(\mathcal{T})$ denotes vector-valued polynomials.

The discrete problem of (2.4)-(2.5) seeks $(\boldsymbol{u}_h, p_h) \in \mathbf{V}_h \times Q_h$ such that

$$\begin{aligned} a(\boldsymbol{u}_h, \boldsymbol{v}_h) + b(p_h, \boldsymbol{v}_h) &= (\boldsymbol{f}, r\boldsymbol{v}_h)_{L_2} \quad \text{for all } \boldsymbol{v}_h \in \mathbf{V}_h \\ b(q_h, \boldsymbol{u}_h) &= 0 \qquad\qquad\quad \text{for all } q_h \in Q_h. \end{aligned} \tag{6.1}$$

Remark 6.1 (Toroidal finite elements)**.** Via the transformation from Cartesian to cylindrical coordinates and vice versa, the discrete spaces $\mathbf{V}_h$ and Q_h can be transformed into toroidal finite element function spaces for the velocity, namely

$$\begin{aligned} \widehat{\mathbf{V}}_h &:= \{\widehat{\boldsymbol{v}}_h : \boldsymbol{v}_h \in \mathbf{V}_h\} \\ &= \{v_{h,r}(r,z)\cos\theta \boldsymbol{e}_x + v_{h,r}(r,z)\sin\theta \boldsymbol{e}_y + v_{h,z}(r,z)\boldsymbol{e}_z : (v_{h,r}, v_{h,z}) \in \mathbf{V}_h\}. \end{aligned}$$

and the pressure space

$$\widehat{Q}_h := \{\widehat{q}_h : q_h \in Q_h\}.$$

The finite element pair is assumed to satisfy the inf-sup condition either in the two-dimensional ansatz spaces $\mathbf{V}_h \times Q_h$ or, equivalently, in the toroidal spaces $\widehat{\mathbf{V}}_h \times \widehat{Q}_h$, i.e. there exists some β_h with

$$\begin{aligned} 0 < \beta_h &\le \inf_{q_h \in Q_h \setminus \{0\}} \sup_{\boldsymbol{v}_h \in \mathbf{V}_h \setminus \{\mathbf{0}\}} \frac{b(\boldsymbol{v}_h, q_h)}{\|q_h\|_{L^2_1(\Omega)} |||\boldsymbol{v}_h|||} \\ &= \inf_{\widehat{q}_h \in \widehat{Q}_h \setminus \{0\}} \sup_{\widehat{\boldsymbol{v}}_h \in \widehat{\mathbf{V}}_h \setminus \{\mathbf{0}\}} \frac{\int_\Omega \operatorname{div}_x \widehat{\boldsymbol{v}}_h \widehat{q}_h \,\mathrm{d}x}{\|\widehat{q}_h\|_{L^2(D)} \|\widehat{\boldsymbol{v}}_h\|_{H^1(D)}}. \end{aligned}$$

Then, the discrete problem (6.1) is uniquely solvable and it holds a best-approximation estimate of the form

$$|||\boldsymbol{u} - \boldsymbol{u}_h||| + \mu^{-1}\|p - p_h\|_{L^2_1(\Omega)} \lesssim \inf_{\boldsymbol{v}_h \in \mathbf{V}_h} |||\boldsymbol{u} - \boldsymbol{v}_h||| + \mu^{-1} \inf_{q_h \in Q_h} \|p - q_h\|_{L^2_1(\Omega)}. \tag{6.2}$$

A proof of the inf-sup stability for the Taylor–Hood finite element method can be found in [LL11; LL12].

Remark 6.2 (Discrete mass conservation)**.** Recall that $b(\boldsymbol{v}_h, q_h) = -(r\operatorname{div}_{(r,z)}(\boldsymbol{v}_h) + v_{h,r}, q_h)_{L^2} = -(\operatorname{div}_{(r,z)}(r\boldsymbol{v}_h), q_h)_{L^2}$. Classical finite element methods like a Taylor–Hood discretization do not result in a divergence-free solution in the sense that

$$\operatorname{div}_{(r,z)}(r\boldsymbol{u}_h) \in Q_h \quad \text{and} \quad \operatorname{div}_{(r,z)}(r\boldsymbol{u}_h) = 0. \tag{6.3}$$

More importantly, also special classical finite element methods that are usually divergence free for the 2D Cartesian formulation by guaranteeing that $\operatorname{div}_{r,z}(V_h) \subset Q_h$, like the Scott–Vogelius finite element method, cannot achieve (6.3) in the axisymmetric setting. This is due to $\operatorname{div}_{(r,z)}(r\boldsymbol{u}_h) \notin Q_h$ in general. Unfortunately, using $u_{K,\sigma} := \int_\sigma r\,\boldsymbol{u}_h \cdot \boldsymbol{n}_{K,\sigma} \,\mathrm{d}S$ directly in the finite volume method therefore does not satisfy the constraint (3.8) that is required in Theorem 3.3. As a remedy, we suggest a postprocessing of $\boldsymbol{u}_h$ in the next subsection.

6.2. **Divergence-free postprocessing and convergence.** Borrowing ideas from [Mer+16], it is possible to postprocess the solution $r\boldsymbol{u}_h$ by a standard local $H(\operatorname{div})$-conforming interpolation Π into a divergence-free auxiliary field $\Pi(r\boldsymbol{u}_h)$ as follows. To employ this trick, we choose a finite element discretization with a velocity space $(\mathbf{P}_k(\mathcal{T}) \cap \mathbf{V}) \subseteq \mathbf{V}_h$ and a discontinuous pressure space $Q_h := P_{k-1}(\mathcal{T})$. Then, we want to find a divergence-free approximation of $r\boldsymbol{u}_h$ in the Brezzi–Douglas–Marini finite element space

$$\mathrm{BDM}_k(\mathcal{T}) := H(\operatorname{div}, \Omega) \cap \mathbf{P}_k(\mathcal{T}).$$

Due to the commutating properties of the standard interpolation Π_{BDM_k}, see e.g. [BBF13, Sec. 2.5.1] for details, it holds

$$0 = \int_\Omega \operatorname{div}_{(r,z)}(r\boldsymbol{u}_h) q_h \,\mathrm{d}r\,\mathrm{d}z = \int_\Omega \operatorname{div}_{(r,z)}(\Pi_{\mathrm{BDM}_k}(r\boldsymbol{u}_h)) q_h \,\mathrm{d}r\,\mathrm{d}z \quad \text{for all } q_h \in Q_h.$$

Since $\operatorname{div}_{(r,z)}(\Pi_{\mathrm{BDM}_k}(r\boldsymbol{u}_h)) \in Q_h$, this implies

$$\operatorname{div}_{(r,z)}(\Pi_{\mathrm{BDM}_k}(r\boldsymbol{u}_h)) = 0. \tag{6.4}$$

For elements with continuous pressure spaces such as the Taylor–Hood element, more involved reconstruction operators Π are available [Led+17]. An element that fits into the framework with discontinuous pressure spaces and $k = 1$ is discussed in the next section. Extensions to higher order $k > 1$ are straightforward. Due to (6.4) the following proposition is straightforward.

Proposition 6.3. Replacing the convective fluxes in (3.4) by

$$u_{K,\sigma} := \int_\sigma \Pi_{\mathrm{BDM}_k}(r\,\boldsymbol{u}_h) \cdot \boldsymbol{n}_{K,\sigma}\,\mathrm{d}S, \tag{6.5}$$

the finite volume divergence constraint (3.8) in Theorem 3.3 is satisfied.

Remark 6.4 (Convergence of the coupled scheme)**.** The replacement of $\boldsymbol{u}$ in (3.4) by $\boldsymbol{u}_h$ and the postprocessing of $r\boldsymbol{u}_h$ by $\Pi_{\mathrm{BDM}_k}(r\boldsymbol{u}_h)$ in (6.5) leads to the error term

$$\begin{aligned}\mathrm{E}(h) := u_{K,\sigma} - \int_\sigma r\,\boldsymbol{u}\cdot\boldsymbol{n}_{K,\sigma}\,\mathrm{d}S &= \int_\sigma (\Pi_{\mathrm{BDM}_k} - 1)(r\,\boldsymbol{u}_h)\cdot\boldsymbol{n}_{K,\sigma}\,\mathrm{d}S \\ &\quad + \int_\sigma r\,(\boldsymbol{u}_h - \boldsymbol{u})\cdot\boldsymbol{n}_{K,\sigma}\,\mathrm{d}S.\end{aligned}$$

With the help of (weighted) trace identities as in [CGP08], standard interpolation estimates and the error estimates (6.2), one can show that $E(h) \to 0$ for $h \to 0$, which ensures the convergence of the coupled scheme.

6.3. **Bernardi–Raugel finite element method.** The Bernardi–Raugel finite element pair is of order $k = 1$ with pressure ansatz space $Q_h := P_0(\mathcal{T})$ and velocity ansatz space

$$\mathbf{V}_h := S_0^1(\mathcal{T})^2 \oplus \{b_F\boldsymbol{n}_F : F \in \mathcal{F}\}$$

where $S_0^1(\mathcal{T}) := \mathbf{P}_1(\mathcal{T}) \cap \mathbf{H}_0^1(\Omega)$ are the continuous piecewise affine functions and b_F is the quadratic face bubble on the face $F \in \mathcal{F}$ of the triangulation $\mathcal{T}$.

The inf-sup stability in the axisymmetric formulation can be shown in a similar way as the inf-sup stability for the Taylor–Hood element in [LL11; LL12], which is briefly discussed for completeness. The main goal is the construction of a Fortin interpolator $\widehat{I}_F : \widehat{\mathbf{H}}_0^1(\Omega) \to \widehat{\mathbf{V}}_h$ that satisfies

$$\int_\Omega \operatorname{div}_x(\widehat{\boldsymbol{v}} - \widehat{I}_F\widehat{\boldsymbol{v}})\widehat{q}_h\,dx = 0 \quad \text{for all } \widehat{q}_h \in \widehat{Q}_h.$$

Since the pressure space Q_h consists of piecewise constants, so $\widehat{Q}_h$ also consists of piecewise constants with respect to the set of toroids $\widehat{\mathcal{T}}$. For the characteristic function $\widehat{\lambda}_{\widehat{T}}$ for such a toroid $\widehat{T} \in \widehat{\mathcal{T}}$, the divergence theorem yields

$$\int_{\widehat{T}} \operatorname{div}_x(\widehat{\boldsymbol{v}} - \widehat{I}_F\widehat{\boldsymbol{v}})\widehat{\lambda}_{\widehat{T}}\,\mathrm{d}x = \int_{\partial\widehat{T}} (\widehat{\boldsymbol{v}} - \widehat{I}_F\widehat{\boldsymbol{v}})\cdot\widehat{\boldsymbol{n}}\,\mathrm{d}S \quad \text{for all } \widehat{\lambda}_{\widehat{T}} \in \widehat{Q}_h.$$

The boundary of $\widehat{T}$ consists of three surfaces that are generated by rotating the three faces of the triangle $T \in \mathcal{T}$ around Γ_{rot}. The goal is to construct the Fortin interpolator such that the boundary integral above vanishes on each face.

As usual, the construction utilizes a quasi-interpolation operator $\widehat{J}$ for the linear part of the velocity ansatz space, e.g. Scott–Zhang type quasi-interpolators for each component as in [LL11, Sec. 2.2.1]. These operators, called $\Pi^+ : H_+^1(\Omega) \to S_0^1(\mathcal{T})$ and $\Pi^- : H_-^1(\Omega) \to S_0^1(\mathcal{T})$, preserve boundary conditions and

exactly interpolate piecewise affine polynomials. In [LL11, Lemmas A.6, A.7] it is shown that

$$\begin{aligned}
\|\Pi^{\pm} v\|_{L_1^2(T)} &\lesssim h_T |v|_{H_1^1(\omega_T)} + \|v\|_{L_1^2(\omega_T)} \\
|\Pi^{\pm} v|_{H_1^1(T)} &\lesssim |v|_{H_1^1(\omega_T)} + h_T^{-1} \|v\|_{L_1^2(\omega_T)} \\
\|v - \Pi^{+} v\|_{L_1^2(T)} &\lesssim h_T |v|_{H_1^1(\omega_T)} \quad \text{for all } v \in H_1^1(\Omega) \\
\|v - \Pi^{-} v\|_{L_1^2(T)} &\lesssim h_T \left(|v|_{H_1^1(\omega_T)} + \|v\|_{L_{-1}^2(\Omega)} \right) \quad \text{for all } v \in H_1^1(\Omega) \cap L_{-1}^2(\Omega)
\end{aligned}$$

where ω_T is some neighbourhood of T.

Due to overlap arguments and the identities

$$\|\widehat{\boldsymbol{v}}\|_{L^2(\Omega)}^2 = 2\pi \left(\|v_r\|_{L_1^2(\Omega)}^2 + \|v_z\|_{L_1^2(\Omega)}^2 \right) \tag{6.6}$$

$$|\widehat{\boldsymbol{v}}|_{H^1(\Omega)}^2 = 2\pi \left(|v_r|_{H_1^1(\Omega)}^2 + \|v_r\|_{L_{-1}^2(\Omega)}^2 + |v_z|_{H_1^1(\Omega)}^2 \right) \tag{6.7}$$

the operator

$$\widehat{J}\widehat{\boldsymbol{v}} := \begin{pmatrix} (\Pi^{-} v_r)\cos(\theta) \\ (\Pi^{-} v_r)\sin(\theta) \\ \Pi^{+} v_z \end{pmatrix}$$

has the following approximation and stability properties.

Lemma 6.5. For any $\widehat{\boldsymbol{v}} \in \mathbf{H}^1(\Omega)$, it holds

$$\|\widehat{\boldsymbol{v}} - \widehat{J}\widehat{\boldsymbol{v}}\|_{L^2(\Omega)} \lesssim h \|\widehat{\boldsymbol{v}}\|_{H^1(\Omega)} \quad \text{and} \quad \|\widehat{J}\widehat{\boldsymbol{v}}\|_{H^1(\Omega)} \lesssim \|\widehat{\boldsymbol{v}}\|_{H^1(\Omega)}.$$

Proof. This follows from the identities (6.6) and (6.7) and the properties of Π^{+} and Π^{-}. Indeed, it holds

$$\begin{aligned}
\|\widehat{\boldsymbol{v}} - \widehat{J}\widehat{\boldsymbol{v}}\|_{L^2(\Omega)}^2 &= 2\pi \left(\|v_r - \Pi^{-} v_r\|_{L_1^2(\Omega)}^2 + \|v_z - \Pi^{+} v_z\|_{L_1^2(T)}^2 \right) \\
&\lesssim 2\pi h^2 \left(|v_r|_{H_1^1(\Omega)}^2 + \|v_r\|_{L_{-1}^2(\Omega)}^2 + |v_z|_{H_1^1(\Omega)}^2 \right) = h^2 \|\widehat{\boldsymbol{v}}\|_{H^1(\Omega)}.
\end{aligned}$$

□

The coefficients α_F for the (toroidal) face bubbles in the definition

$$\widehat{I}_F \widehat{\boldsymbol{v}} := \widehat{J}\widehat{\boldsymbol{v}} + \sum_{F \in \mathcal{F}} \alpha_F \widehat{b}_F \widehat{\boldsymbol{n}}_F$$

can be adjusted straightforwardly to correct the normal fluxes, i.e., by

$$\alpha_F := \frac{\int_{\widehat{F}} (\widehat{J}\widehat{\boldsymbol{v}} - \widehat{\boldsymbol{v}}) \cdot \widehat{\boldsymbol{n}}_F \, \mathrm{d}S}{\int_{\widehat{F}} \widehat{b}_F \, \mathrm{d}S} \quad \text{such that} \quad \int_{\widehat{F}} (\widehat{I}_F \widehat{\boldsymbol{v}} - \widehat{\boldsymbol{v}}) \cdot \widehat{\boldsymbol{n}}_F \, \mathrm{d}S = 0.$$

This shows that $\widehat{I}_F$ is a Fortin interpolator, which is equivalent to the existence of $\beta_h > 0$ in the inf-sup stability condition via classical mixed finite element theory, see e.g. [BBF13, Proposition 5.4.2].

Remark 6.6 (P2–Bubble finite element method)**.** In [Rua03], it is shown that a second-order element, i.e. $k = 2$, based on the pressure space $Q_h := P_1(\mathcal{T})$ and the velocity ansatz space

$$\mathbf{V}_h := S_0^2(\mathcal{T})^2 \oplus \{ b_T \boldsymbol{e}_j : T \in \mathcal{T}, j \in \{1,2\} \},$$

which consists of continuous quadratic polynomials enriched with cell bubbles b_T, is also inf-sup stable in the axisymmetric setting.

7. Numerical Examples

This section discusses some experiments to study the convergence behaviour of the scheme and to demonstrate its mass conservative features, in particular when a discrete velocity and the postprocessing from (6.2) is used.

Remark 7.1 (On other convection-difffusion flux discretizations)**.** The theory in this paper only covers the classical upwinding flux, but other flux discretizations are also frequently used. One example is the exponentially-fitted or Scharfetter–Gummel two-point flux approximation that replaces $F_{K,\sigma} + V_{K,\sigma}$ by

$$F_{K,\sigma} := \tau_\sigma \left(B\left(\frac{u_\sigma}{D}\right) c_K - B\left(-\frac{u_\sigma}{D}\right) c_L \right) \quad \text{where} \quad u_\sigma := \int_\sigma \boldsymbol{u} \cdot (\boldsymbol{x}_K - \boldsymbol{x}_L)\, \mathrm{d}S,$$

which involves the local Péclet number $\mathrm{Pe}_\sigma := u_\sigma / D$ as an argument for the Bernoulli function $B(x) := x/(e^x - 1)$. A proof of min/max principles, stability and convergence for the present model problem in the Cartesian setting can be found e.g. in [FLL11a]. Improved second order L^2 error estimates can be shown on special families of structured meshes, see e.g. the seminal papers by [Ili69; SG69] as well as [DN18] and the references therein for more details. A thorough investigation of the error analysis extended to cylindrical coordinates is beyond the scope of the paper. However, experimentally one observes optimal L^2 error convergence rates also on more general families of triangulations as demonstrated in the first numerical example below. In all other experiments only the exponential fitting flux discretization is used.

Remark 7.2 (Implementation issues)**.** Note, that the computation of (6.5) requires integration along the boundary edges σ of the finite volume control volumes, which in general do not and need not match edges of the finite element mesh. Hence, an algorithm is required that computes the intersections of σ with the triangles of the finite element mesh. Some aspects for the Cartesian setting even in three dimensions are discussed in [FLL11a, Sec. 5.2]. For the two-dimensional axisymmetric setting the situation is even simpler.

An implementation is available in `julia` as an extension for the finite volume method from `VoronoiFVM.jl`, see [Fuh+25] that allows to couple velocity fields from the finite element method package

`ExtendableFEM.jl` [Mer+25].

7.1. **Convergence studies.** The first example studies the combination of the finite volume method and the finite element method for the prescribed analytic solution

$$c(r,z) := r^3 \quad \text{and} \quad \boldsymbol{u}(r,z) := \frac{1}{H^2}(H^2 - r^2)$$

with parameter $D = 1$.

Figure 7.1 (left) compares the convergence histories for the errors $\|c - c_h\|_{1,\mathcal{K}}$ of the discrete finite volume solution c_h for various choices of the velocity for the convection term: the exact velocity $\boldsymbol{u}$, and approximations $\boldsymbol{u}_h$ via the Bernardi–Raugel finite element method with and without the divergence-free postprocessing at various levels of refinement for the approximation of $\boldsymbol{u}_h$. It can be seen that the finite volume error converges optimally until the error from the Stokes discretization on the coarsest mesh ($n_{\text{ref}} = 1$) is too large. If the mesh size for the Stokes problem is uniformly refined two more times ($n_{\text{ref}} = 3$) such that the error from the Stokes problem is much smaller, the finite volume error continues to converge optimally as well. The order of convergence is in line with the theoretical results of Theorem 4.5. We also observe that the results for the non-postprocessed velocity are worse than for the postprocessed velocity at the same refinement level. This indicates that the postprocessing is not only beneficial for the maximum principle, but also for the accuracy of the finite volume solution in the natural norms.

Figure 7.1 (right) also displays the convergence history of the Stokes problem (pressure p_h and velocity $\boldsymbol{u}_h$) computed on the Delaunay triangulation $\mathcal{T}$ that generated the control volumes $\mathcal{K}$ for the finite volume scheme. The plots confirm the optimal first-order convergence in accordance with (6.2).

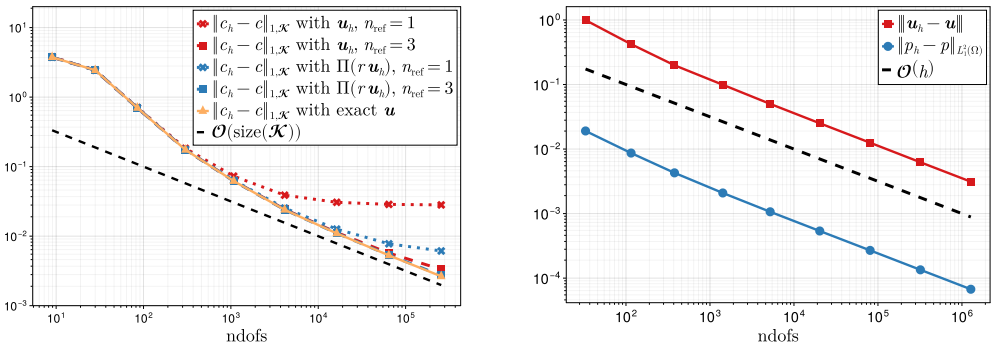

FIGURE 7.1. Example in Section 7.1: Comparison of convergence rates for the axisymmetric finite volume approximation c_h of $c(r,z) = r^3$ with various choices for the velocity $\boldsymbol{u}_h$ (left) and convergence rate of the finite element solution $\boldsymbol{u}_h$ to the axisymmetric Stokes problem on the dual Delaunay triangulation $\mathcal{T}$ (right).

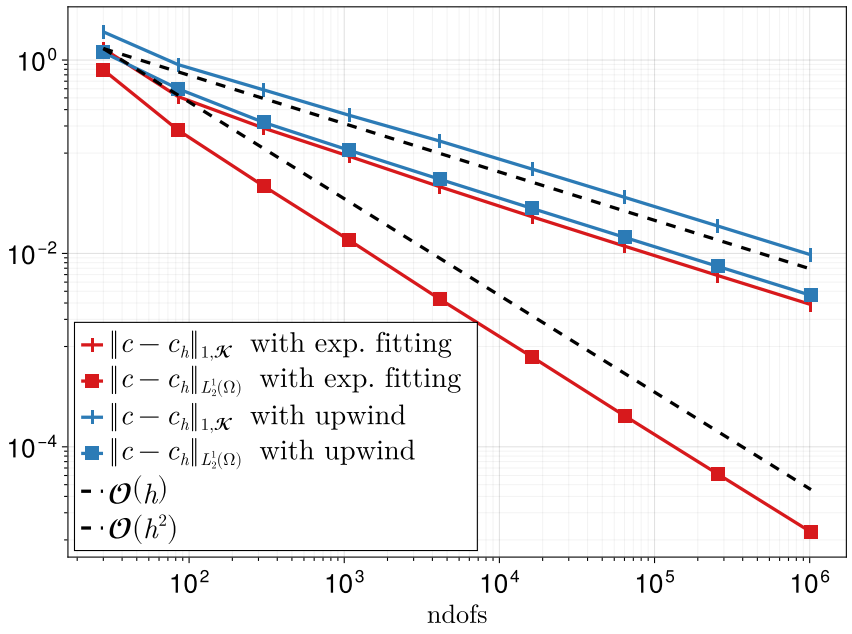

FIGURE 7.2. Example in Section 7.1: Comparison of convergence rates for the axisymmetric finite volume approximation c_h of $c(r,z) = r^3$ with an exact velocity $\boldsymbol{u}_h$ for an upwinding and exponential fitting flux discretization.

In Figure 7.2, we compare the convergence rates of the discrete $H_1^1(\Omega)$ and $L_1^2(\Omega)$ errors for the upwind flux and the exponential fitting flux discretization from Remark 7.1. As one can see, the exponential fitting flux is able to obtain a second-order convergence in the $L_1^2(\Omega)$ error norm.

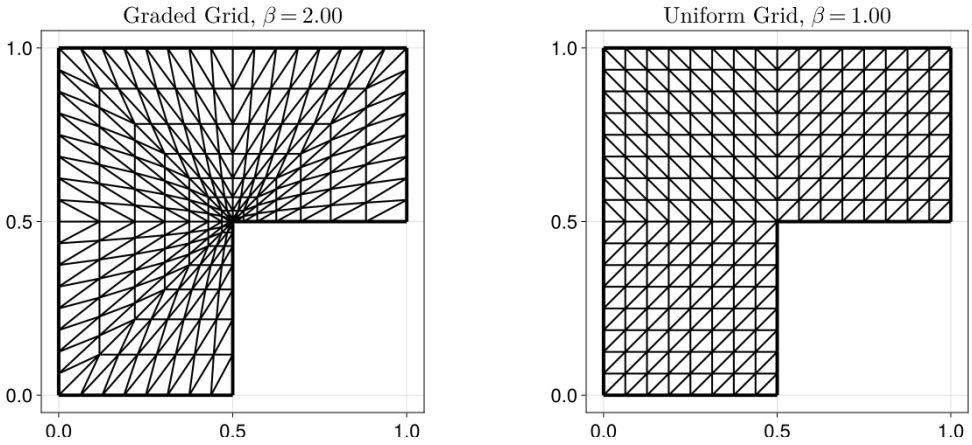

FIGURE 7.3. Example in Section 7.2: Graded mesh for the L-shaped domain with $\beta = 2$ (left) and a uniform mesh ($\beta = 1$).

7.2. **L-shaped domain.** The second example investigates the convergence order of the finite element method for the Stokes problem on an L-shaped domain on graded meshes to experimentally confirm two expectations. First, optimal convergence orders for the Stokes discretizations are possible with graded meshes as investigated in [LL12] for the Taylor–Hood family. Second, severe violations of the maximum principle are demonstrated for the coupled scheme without the postprocessed velocity field.

Figure 7.3 displays a graded mesh and a uniformly structured mesh for the L-shaped domain $\Omega := (0,1)^2 \setminus ([0.5,1.0] \times [0.0,0.5])$. The grading towards the reentrant corner $(0.5, 0.5)$ is done via β-grading, which involves the function $g(s) = s^\beta$, where s is the distance to the reentrant corner, to reposition nodes on all rays towards the reentrant corner.

Figure 7.4 shows the convergence history of the error $|||\boldsymbol{u} - \boldsymbol{u}_h|||$ where $\boldsymbol{u}$ is a reference solution, which is obtained by a Taylor–Hood method on a similarly graded, but much finer mesh. It is confirmed that the optimal error rate can be achieved on reasonably graded meshes. On uniform meshes, only suboptimal convergence rates of about $\mathcal{O}(h^{0.56})$ are obtained, which is very close to the expected rates from theory and similar experiments for the Cartesian case [BR81; Ver89].

The optimal grid for $\beta = 2$ is then used for the transport simulation with an inlet $\Gamma_{\text{in}} = [0, 0.5] \times \{0\}$, where Dirichlet conditions are enforced, and homogeneous Neumann conditions on the rest of the boundary. The inlet concentration is set to $c_{\text{in}} = 1.0$. The exact solution should be constant, i.e., $c \equiv 1.0$. However, any error in the (axisymmetric) divergence of the discrete velocity field may cause deviations from this expected value. Figure 7.5 displays those errors for a simulation with $D = 10^{-5}$, where we observe violations up to $6 \cdot 10^{-2}$. Surprisingly, violations are not only located close to the reentrant corner, but also at the opposite wall close to the axis of revolution.

7.3. **Lévêque asymptotics.** In our final example, we investigate if the finite volume method is able to preserve a known analytic asymptotic expression. The following Lévêque problem goes back to [Fuh+08] and studies the transport equation for $D = 1$ on a tubular channel domain with radius $R = 2$ of a length $L = 10$, and with an electrode along the outer wall with a length $L_{\text{el}} = 6$, i.e. $\Omega := (0, R) \times (0, L)$. We specify an inlet concentration of $c_{\text{in}} = 1$ along $\Gamma_{\text{in}} := (0, R) \times \{0\}$ and Dirichlet boundary condition $c_{\text{el}} = 0$ on the electrode boundary $\Gamma_{\text{el}} := \{R\} \times (2, L - 2)$ mimicking a fast reaction that consumes the

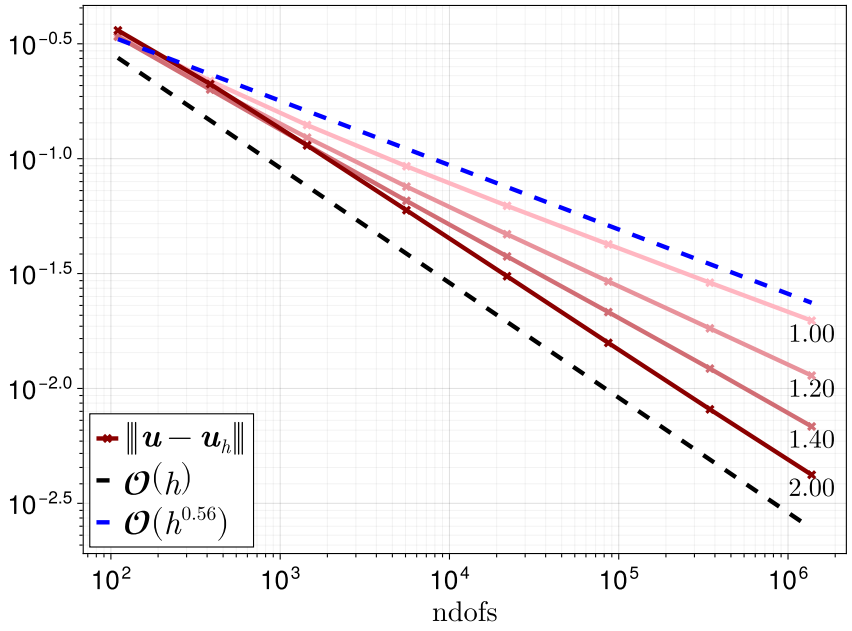

FIGURE 7.4. Example in Section 7.2: Convergence history of the discrete velocity error for different choices of the grading parameter β.

species. The velocity field is given by the typical Hagen-Poiseuille channel flow profile

$$\boldsymbol{u}(r,z) := \frac{\mathrm{Pe}\, D}{R}\left(1-\frac{r^2}{R^2}\right)\cdot[0,1]^T$$

scaled by the Péclet number $\mathrm{Pe} = 2Ru_{\max}/D$, where $u_{\max}$ is the maximum flow velocity. At the outflow boundary $\Gamma_{\text{out}} := (0,R)\times\{L\}$ do-nothing boundary conditions are employed, while to the rest of the boundary, in particular the axis of revolution, homogeneous Neumann boundary conditions are applied. Newman [New69] computed an asymptotic expression for the resulting Sherwood number Sh, which is expressed as the ratio of convective mass transfer to diffusive mass transfer, namely

$$\mathrm{Sh} := \frac{J}{\pi\, L_{\text{el}}\, D\,(c_{\text{in}}-c_{\text{el}})} \quad \text{with} \quad J := 2\pi\int_{\Gamma_{\text{el}}} r\,\boldsymbol{j}(c)\cdot\boldsymbol{n}\,\mathrm{d}S. \tag{7.1}$$

In the limit of convection-dominated flow (with high Pe), we then expect

$$\mathrm{Sh} \approx 1.6151\left(\frac{\mathrm{Pe}}{z/(2R)}\right)^{1/3}. \tag{7.2}$$

The example allows to test the correct quantitative behavior in boundary layers. Accuracy in such a scenario is crucial in closely-related models, e.g. in heterogeneous catalysis to infer correct reaction rates.

Figure 7.6 compares the expected asymptotic relationship (7.2) between the Sherwood and Péclet numbers where the Sherwood number is computed according to (7.1) from the discrete electrode current $J(c_h)$ of the discrete finite volume solution c_h via a test function approach in accordance with [FLL11a, Sec. 4.1] on a very fine computational grid that is strongly refined towards the expected boundary layer at the electrode, see e.g. [Fuh+08].

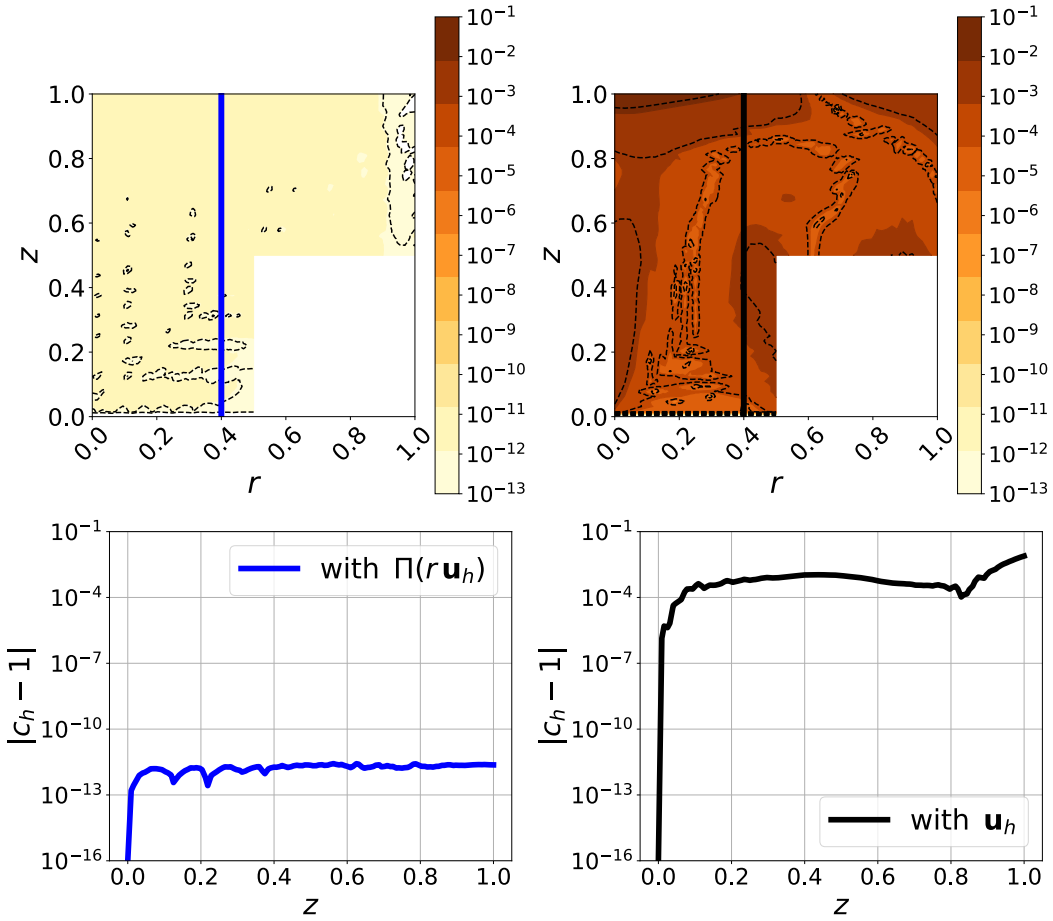

FIGURE 7.5. Example in Section 7.2: Error between the computed species concentration c_h and the exact concentration $c \equiv c_{\text{in}} = 1$ in the domain (top) and along the line $\{0.4\} \times (0, 1)$ (bottom) when the postprocessed velocity (left) or the non-postprocessed velocity field (right) is used in the case $D = 10^{-5}$.

It can be seen that the asymptotic behaviour agrees with the expected behaviour for a very large range of Péclet numbers, similar to the experiments in [Fuh+08]. However, there are significant differences with respect to the chosen discretization of the convection term. The best results are obtained when the exact analytical velocity field is used in the computation of (3.4). The worst results are obtained when the unpostprocessed Bernardi–Raugel finite element approximation $\boldsymbol{u}_h$ is used. The results can be improved such that the asymptotics are preserved for up to about one more magnitude larger Pe by the reconstruction procedure that replaces the convective fluxes by (6.5).

REFERENCES

[BBD06] Zakaria Belhachmi, Christine Bernardi, and Simone Deparis. “Weighted Clément operator and application to the finite element discretization of the axisymmetric Stokes problem”. en. In: *Numerische Mathematik* 105.2 (Nov. 2006), pp. 217–247. ISSN: 0029-599X, 0945-3245. DOI: 10.1007/s00211-006-0039-9.

[BBF13] D. Boffi, F. Brezzi, and M. Fortin. *Mixed Finite Element Methods and Applications*. Springer Series in Computational Mathematics. Springer Berlin Heidelberg, 2013. ISBN: 9783642365195.

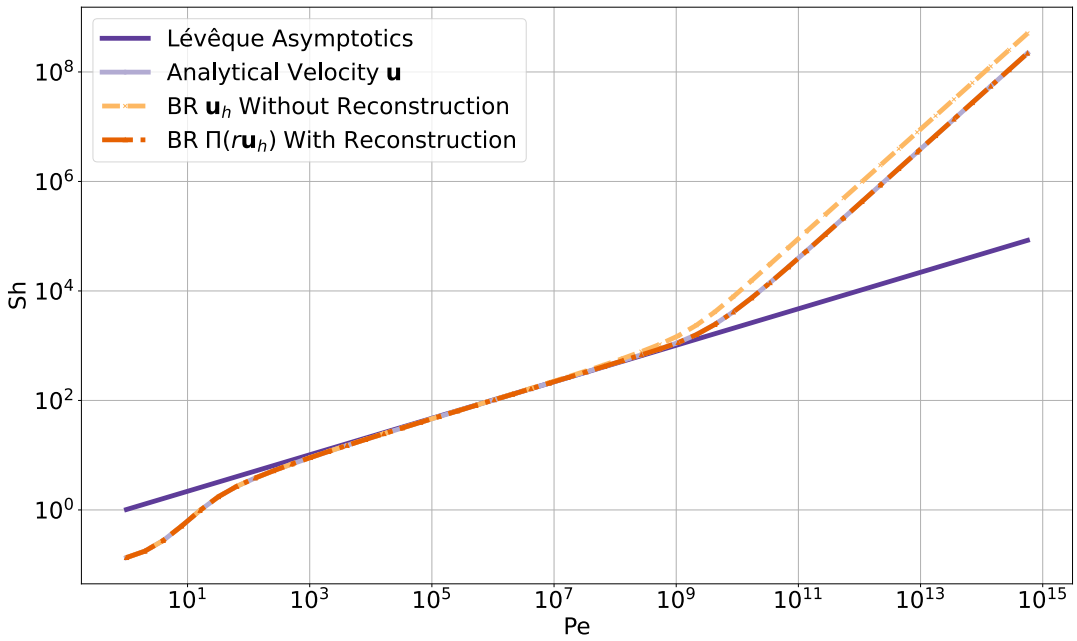

FIGURE 7.6. Example in Section 7.3: Comparison of the Sherwood number in relation to the Péclet number for solutions to (5.1) with reconstructed and non-reconstructed FEM approximations of the velocity $\boldsymbol{u}_h$.

[BDM99] Christine Bernardi, Monique Dauge, and Yvon Maday. *Spectral Methods for Axisymmetric Domains*. Vol. 3. Gauthier-Villars, Jan. 1999.

[BFO96] Barry Bernstein, Kathleen A. Feigl, and Elwood T. Olsen. "A First-Order Exactly Incompressible Finite Element for Axisymmetric Fluid Flow". In: *SIAM Journal on Numerical Analysis* 33.5 (1996), pp. 1736–1758. DOI: 10.1137/S0036142994243095.

[BR81] C. Bernardi and G. Raugel. "Mixed finite element method for the Stokes and Navier-Stokes equations in a nonconvex polxgon". French. In: *Calcolo* 18 (1981), pp. 255–291. ISSN: 0008-0624. DOI: 10.1007/BF02576359.

[BR85] Christine Bernardi and Geneviève Raugel. "Analysis of some finite elements for the Stokes problem". In: *Math. Comp.* 44.169 (1985), pp. 71–79. ISSN: 0025-5718.

[Bra07] Dietrich Braess. *Finite elements - Theory, fast solvers, and applications in solid mechanics*. New York: Cambridge University Press, 2007.

[CCG08] Caterina Calgaro, Emmanuel Creusé, and Thierry Goudon. "An Hybrid Finite Volume-Finite Element Method for Variable Density Incompressible Flows". In: *Journal of Computational Physics* 227.9 (Apr. 2008). Publisher: Elsevier, pp. 4671–4696. DOI: 10.1016/j.jcp.2008.01.017.

[CGP08] Dylan M. Copeland, Jayadeep Gopalakrishnan, and Joseph E. Pasciak. "A mixed method for axisymmetric div-curl systems". en. In: *Mathematics of Computation* 77.264 (Mar. 2008), pp. 1941–1965. ISSN: 0025-5718. DOI: 10.1090/S0025-5718-08-02102-9.

[DN18] Jerome Droniou and Neela Nataraj. "Improved L^2 estimate for gradient schemes, and superconvergence of the TPFA finite volume scheme". In: *IMA Journal of Numerical Analysis* 38.3 (July 2018), pp. 1254–1293. ISSN: 0272-4979, 1464-3642. DOI: 10.1093/imanum/drx028.

[EGH00] R. Eymard, T. Gallouët, and R. Herbin. "Finite volume methods". In: *Handbook of numerical analysis, Vol. VII*. North-Holland, 2000, pp. 713–1020.

[EJ13] V.J. Ervin and E.W. Jenkins. “Stenberg’s sufficiency criteria for the LBB condition for axisymmetric Stokes flow”. In: *Journal of Mathematical Analysis and Applications* 398.1 (2013), pp. 421–437. ISSN: 0022-247X. DOI: https://doi.org/10.1016/j.jmaa.2012.09.003.

[Eym+07] R. Eymard et al. “Analysis tools for finite volume schemes”. In: *Acta Math. Univ. Comenian. (N.S.)* 76.1 (2007), pp. 111–136. ISSN: 0862-9544.

[FLL11a] J. Fuhrmann, A. Linke, and H. Langmach. “A numerical method for mass conservative coupling between fluid flow and solute transport”. In: *Appl. Num. Math.* 61.4 (2011), pp. 530–553.

[FLL11b] Jürgen Fuhrmann, Alexander Linke, and Hartmut Langmach. “A numerical method for mass conservative coupling between fluid flow and solute transport”. en. In: *Applied Numerical Mathematics* 61.4 (Apr. 2011). Number: 4, pp. 530–553. ISSN: 01689274. DOI: 10.1016/j.apnum.2010.11.015.

[Fuh+08] J. Fuhrmann et al. “Experimental and numerical model study of the limiting current in a channel flow cell with a circular electrode”. In: *Phys. Chem. Chem. Phys.* 10 (25 2008), pp. 3784–3795.

[Fuh+25] Jürgen Fuhrmann et al. *VoronoiFVM.jl - Finite volume solver for coupled nonlinear partial differential equations*. Version v2.12.2. Aug. 2025. DOI: 10.5281/zenodo.16689646.

[GH05] Emily Gallouët and Raphaèle Herbin. “Axisymmetric finite volumes for the numerical simulation of bulk CO 2 transport and assimilation in a leaf”. In: *International Journal On Finite Volumes* 2.2 (Jan. 2005).

[GHV00] Thierry Gallouët, Raphaèle Herbin, and Marie Hélène Vignal. “Error Estimates on the Approximate Finite Volume Solution of Convection Diffusion Equations with General Boundary Conditions”. In: *SIAM Journal on Numerical Analysis* 37.6 (2000), pp. 1935–1972. DOI: 10.1137/S0036142999351388.

[GR86] V. Girault and P.-A. Raviart. *Finite Element Methods for Navier-Stokes Equations*. Vol. 5. Springer Series in Computational Mathematics. Berlin: Springer-Verlag, 1986.

[Ili69] A. M. Il’in. “A difference scheme for a differential equation with a small parameter multiplying the second derivative”. In: *Mat. zametki* 6 (1969), pp. 237–248.

[Joh+17] Volker John et al. “On the Divergence Constraint in Mixed Finite Element Methods for Incompressible Flows”. In: *SIAM Review* 59.3 (2017), pp. 492–544. DOI: 10.1137/15M1047696.

[KP05] Olaf Klein and Peter Philip. “Transient conductive–radiative heat transfer: discrete existence and uniqueness for a finite volume scheme”. In: *Mathematical Models and Methods in Applied Sciences* 15.02 (2005), pp. 227–258. DOI: 10.1142/S0218202505000340.

[Kuf85] Alois Kufner. “Weighted Sobolev Spaces”. In: 1985.

[Led+17] Philip L. Lederer et al. “Divergence-free Reconstruction Operators for Pressure-Robust Stokes Discretizations with Continuous Pressure Finite Elements”. In: *SIAM Journal on Numerical Analysis* 55.3 (2017), pp. 1291–1314. DOI: 10.1137/16M1089964.

[Liu+25] Xuefeng Liu et al. “Rectangular divergence-free finite elements for axisymmetric Stokes equations”. In: *Journal of Scientific Computing* 105 (Oct. 2025). DOI: 10.1007/s10915-025-03094-7.

[LL11] Young-Ju Lee and Hengguang Li. “On Stability, Accuracy, and Fast Solvers for Finite Element Approximations of the Axisymmetric Stokes Problem by Hood–Taylor Elements”. In: *SIAM Journal on Numerical Analysis* 49.2 (2011), pp. 668–691. DOI: 10.1137/100783339.

[LL12] Young-Ju Lee and Hengguang Li. “Axisymmetric Stokes equations in polygonal domains: Regularity and finite element approximations”. In: *Computers & Mathematics with Applications* 64.11 (2012), pp. 3500–3521. ISSN: 0898-1221. DOI: https://doi.org/10.1016/j.camwa.2012.08.014.

[Mer+16] C. Merdon et al. “Inverse modeling of thin layer flow cells for detection of solubility, transport and reaction coefficients from experimental data”. In: *Electrochimica Acta* 211 (2016), pp. 1–10.

ISSN: 0013-4686. DOI: https://doi.org/10.1016/j.electacta.2016.05.101.

[Mer+25] Christian Merdon et al. *ExtendableFEM.jl*. Version v1.5.0. Sept. 2025. DOI: 10.5281/zenodo.17199755.

[New69] John Newman. “Extension of the Lévêque Solution”. In: (1969).

[Phi03] P. Philip. “Transient Numerical Simulation of Sublimation Growth of SiC Bulk Single Crystals: Modeling, finite volume method, results”. Weierstraß-Institut für Angewandte Analysis und Stochastik, 2003. DOI: https://doi.org/10.20347/WIAS.REPORT.22.

[Rua03] Vitoriano Ruas. “Mixed finite element methods with discontinuous pressures for the axisymmetric Stokes problem”. In: *ZAMM Z. Angew. Math. Mech.* 83.4 (2003), pp. 249–264. ISSN: 0044-2267,1521-4001. DOI: 10.1002/zamm.200310032.

[SG69] D. L. Scharfetter and H. K. Gummel. “Large signal analysis of a silicon Read diode”. In: *IEEE Trans. Electron. Dev.* 16 (1969), pp. 64–77.

[Ver89] R Verfürth. “A posteriori error estimators for the Stokes equations”. In: *Numerische Mathematik* 55.33 (1989), pp. 309–325. DOI: 10.1007/BF01390056.